NJC

New Journal of Chemistry

A journal for new directions in chemistry

Accepted Manuscript

This article can be cited before page numbers have been issued, to do this please use: J. C. P. Mayer, T. Acunha, O. E. D. Rodrigues, D. F. Back, O. A. Chaves, L. Dornelles and B. A. Iglesias, *New J. Chem.*, 2020, DOI: 10.1039/D0NJ04530F.

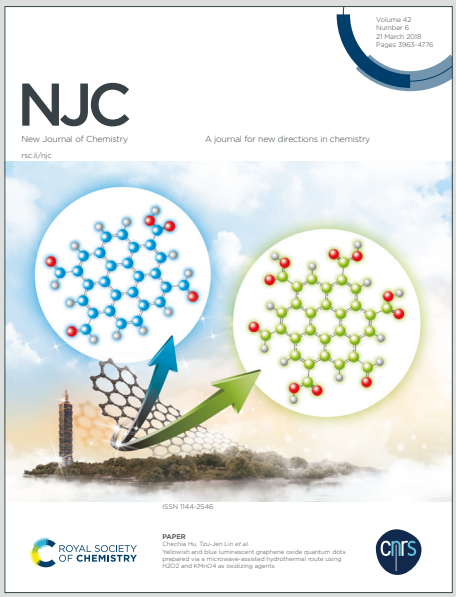

Synthesis, spectroscopic characterization and DNA/HSA binding study of (phenyl/naphthyl)ethenyl-substituted 1,3,4-oxadiazolyl-1,2,4-oxadiazoles

João C. P. Mayer,[a] Thiago V. Acunha,[b] Oscar E. D. Rodrigues,[a] Davi F. Back,[c] Otávio Augusto Chaves,[d] Luciano Dornelles[a]* and Bernardo A. Iglesias[b]**

[a] *Departamento de Química, LabSelen-NanoBio, Universidade Federal de Santa Maria, CEP 97105-900, Santa Maria, RS, Brazil.*

[b] *Departamento de Química, Laboratório de Bioinorgânica e Materiais Porfirínicos, Universidade Federal de Santa Maria, CEP 97105-900, Santa Maria, RS, Brazil.*

[c] *Laboratório de Materiais Inorgânicos - Departamento de Química, CCNE, UFSM, Santa Maria – RS, Brazil, Zip Code 97105-900.*

[d] *Instituto SENAI de Inovação em Química Verde, Rua Morais e Silva N° 53, Bloco 09, CEP 20271030, Rio de Janeiro, RJ, Brazil.*

* Corresponding author.

** Corresponding author.

E-mail adresses: bernardopgq@gmail.com; bernardo.iglesias@ufsm.br (B.A. Iglesias), ldornel@gmail.com (L. Dornelles).

DOI: 10.1039/D0NJ04530F

Abstract

Two new series of conjugated arylethenyl-1,3,4-oxadiazolyl-1,2,4-oxadiazoles were obtained and spectroscopically characterized in terms of UV-Vis absorption, fluorescence and interaction with CT-DNA and Human Serum Albumin (HSA) biomolecules. Phenyl- and 1-naphthyl-bearing examples were analysed, and the spectroscopic properties of its substitution series were compared, showing extensive conjugation in all compounds, and absorption differences due to both aryl-ethenyl subunit and substituted phenyl/phenylene at the 1,2,4-oxadiazole side. Strong binding interaction of the obtained examples with CT-DNA and moderate HSA-association capability were observed spectroscopically, and further docking studies were performed.

Keywords: *1,2,4-oxadiazoles, 1,3,4-oxadiazoles, photophysical properties, DNA binding, HSA binding.*

Introduction

Heterocyclic compounds, in special azoles, have long been object of much attention in chemistry.[1] Among nitrogen-bearing heterocycles, oxadiazoles represent a significant portion of target molecules in organic synthesis.[2] In addition to the methods themselves, focus is given to their pharmacological activities and also to their physical-chemical properties.[3] 1,2,4- And 1,3,4-oxadiazoles are the most described oxadiazole regioisomers, and these have been incorporated in a great number of functional molecules, including antitumor,[4] antiviral[5] and antidepressant drugs,[6] as well as in polymeric species.[7] Moreover, due to its highly conjugated structure, aryl-1,3,4-oxadiazoles and their vinylogous counterparts have often been incorporated in the synthesis of fluorescent compounds.[8]

Molecules containing the di-heterocyclic moiety 1,3,4-oxadiazolyl-1,2,4-oxadiazole have been studied recently by our group, having electron-withdrawing properties associated to the oxadiazoles and displaying significant binding affinity for CT-DNA.[9] However, the fluorescence spectroscopic properties of molecules based on these di-heterocyclic scaffold remained uncharacterized.

View Article Online
DOI: 10.1039/D0NJ04530F

Since there is interest in DNA-binding molecules to be employed as drugs and/ or biochemical probes, fluorescent 1,3,4-oxadiazolyl-1,2,4-oxadiazole derivativatives may deserve attention for the development of such compounds.[10] Considering other results obtained for previous, ferrocene-substituted chemical species,[9] it would be plausible to study any observable fluorescence after replacement of ferrocene by other aryl groups, making fluorescence spectroscopic characterization of the respective DNA and/or protein-compound adducts possible.

In this work, a library of new fluorescent (phenyl/naphthyl)-ethenyl-1,3,4-oxadiazolyl-1,2,4-oxadiazoles (**7aa-be**, Fig. 1) were prepared and fully characterized by analytical techniques. Photophysical properties of these derivatives were evaluated by UV-Vis and steady-state fluorescence emission spectroscopy. Moreover, DNA and HSA binding assays were conducted by spectroscopic and theoretical analysis (molecular docking).

View Article Online
DOI: 10.1039/D0NJ04530F

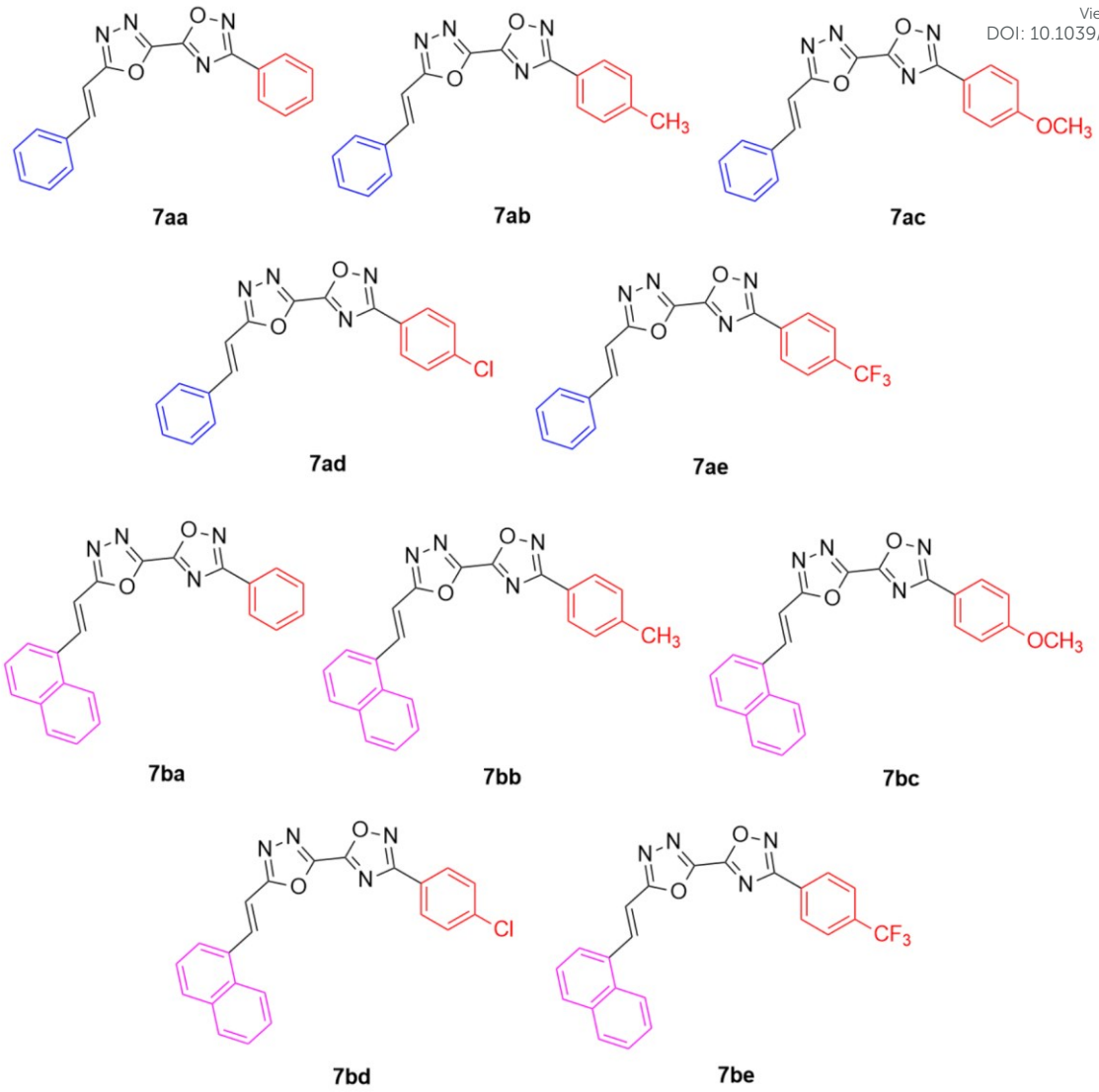

Fig. 1. Structural representation of the 1,3,4-oxadiazolyl-1,2,4-oxadiazoles **7aa-be**.

Experimental

General analysis

High-resolution mass spectra (HRMS) were obtained for compounds **7aa-be** on a XEVO G2-Q-TOF (Waters) mass spectrometer, operating in ESI(+) mode, at the Chemistry Department, Federal University of Santa Maria.

Thin layer chromatography (TLC) was performed using Merck Silica Gel GF_{254}, 0.25 mm. For visualization, TLC plates were either placed under ultraviolet light, or stained with iodine vapor, or acidic vanillin solution followed by heating.

View Article Online
DOI: 10.1039/D0NJ04530F

Proton nuclear magnetic resonance spectra (^{1}H NMR) were obtained at 400 MHz in a Bruker Avance III HD NMR spectrometer. Spectra were recorded in either $CDCl_3$ or DMSO-d_6 solutions. Chemical shifts are reported in ppm, referenced to the solvent peak of tetramethyl silane (TMS) as the external reference. Data are reported as follows: chemical shift (δ) expressed in ppm, multiplicity (br = broad, s = singlet, d = doublet, dd = doublet of doublets, ddd = doublet of doublet of doublets, dt = doublet of triplets, t = triplet, m = multiplet, q = quartet), and coupling constant (*J*) in Hertz and integrated intensity. Carbon-13 nuclear magnetic resonance (^{13}C NMR) spectra were obtained at 100 MHz in an AVANCE III HD NMR spectrometer. Chemical shifts (δ) are reported in ppm, referenced to the solvent peak of $CDCl_3$ or DMSO-d_6. Deuterated solvents were acquired from Cambridge Isotope Laboratories®, having TMS added on opening.

X-Ray crystallography

Crystallographic data were collected on a Bruker D8 Venture Photon 100 diffractometer equipped with an Incoatec IμS high brilliance Mo-Kα X-ray tube with two-dimensional Montel micro-focusing optics. The structure was solved by direct methods using SHELXS.[11] Subsequent Fourier-difference map analyses yielded the positions of the non-hydrogen atoms. Refinements were carried out with the SHELXL package.[11] All refinements were made by full-matrix least-squares on F2 with anisotropic displacement parameters for all non–hydrogen atoms. Hydrogen atoms were included in the refinement in calculated positions but the atoms (of hydrogens) that are commenting performing special bond were located in the Fourier map. Drawings were done using ORTEP for Windows.[12] Crystal data and more details of the data collection and refinements of the ligand in the *support information section* (Figure S31).

Photophysical analysis

Electronic UV-Vis absorption spectra were recorded using Shimadzu UV2600 spectrophotometer (data interval, 1.0 nm) using chloroform and DMSO as solvent. Steady-state fluorescence spectra of samples in $CHCl_3$ and DMSO solutions were measured with a Varian Cary 50 fluorescence spectrophotometer (emission; slit 2.5 mm) and were corrected according to the manufacturer's instructions. Fluorescence quantum yields (Φ_f) of the compounds **7aa-ae/7ba-be** in solutions were determined by

View Article Online
DOI: 10.1039/D0NJ04530F

comparing the corrected fluorescence spectra with 9,10-diphenylanthracene (DPA) in chloroform (Φ_f = 0.65, λ_{ex} = 366 nm) as fluorescence yield standard.[13] Collecting the samples and the standard fluorescence spectra at the same experimental condition, the fluorescence quantum yield was calculated by Equation 1:

$$\Phi_F = \Phi_{F_{std}} \frac{I}{I_{std}} \frac{(1-10^{-A})_{std}}{(1-10^{-A})} \frac{\eta}{\eta_{std}} \quad \textbf{(1)}$$

where Φ_F, I, A and η are the fluorescence quantum yield, the integral area of fluorescence emission, the absorbance in $\lambda_{exc.}$ and refractive index of selected solvents. The subscript *"std"* refers to the standard molecule - in this case, 9,10-diphenylanthracene (**DPA**) (Φ_F = 0.65 in chloroform solution).

CT-DNA binding assays

The interaction between calf-thymus DNA (CT-DNA) and compounds **7aa-ae/7ba-be** were conducted by UV-Vis absorption measurements at room temperature in PBS buffer at pH 7.2, using DMSO stock solution of derivatives (10^{-4} M range) at 300 to 700 nm. The DNA pair base concentrations of low molecular weight DNA from CT-DNA was determined by absorption spectroscopy, using the molar extinction coefficients 6,600 $M^{-1}cm^{-1}$ (per base pair) at λ_{max} = 260 nm. Heterocycle compound solutions in DMSO with PBS buffer were titrated with increasing concentrations of CT-DNA (ranging from 0-100 μM). The intrinsic binding constants (K_b) of derivatives were calculated according to the decay of the absorption bands of compounds using Equation 2, through a plot of [DNA]/($\varepsilon_a - \varepsilon_f$) *versus* [DNA]:

$$\frac{[DNA]}{|(\varepsilon_a - \varepsilon_f)|} = \frac{[DNA]}{|(\varepsilon_b - \varepsilon_f)|} + \frac{1}{K_b|(\varepsilon_b - \varepsilon_f)|} \quad (2)$$

where [DNA] is the concentration of CT-DNA in the base pairs, ε_a is the extinction coefficient (A_{obs}/[compound]), ε_b and ε_f are the extinction coefficients of free and fully bound forms, respectively. In plots of [DNA]/($\varepsilon_a - \varepsilon_f$) *versus* [DNA], K_b is given by the ratio of the slope to the interception.

View Article Online
DOI: 10.1039/D0NJ04530F

Also, the standard Gibbs' free-energy (ΔG^o) of CT-DNA:derivative adduct was calculated from the values of K_b using Equation 3:

$$\Delta G^\circ = -\mathrm{RT}\ln K_b \tag{3}$$

where R and T are the gas constant (1.987 $kcalK^{-1}mol^{-1}$) and temperature (298K), respectively.

The competition binding studies were conducted via steady-state fluorescence emission analysis in the same fluorimeter described in the photophysical analysis. The derivatives **7ba-be** were dissolved in DMSO (stock solution at 10^{-5} M range) and competitive studies were performed through the gradual addition of the compounds to a quartz cuvette (1.0 cm path length) containing ethidium bromide (EB, 2.0×10^{-7} M) and DNA (2.0×10^{-5} M) in a PBS (pH 7.2). The concentration of derivatives ranged from 0 to 100 μM. Compounds were excited at λ_{exc} = 510 nm and steady-state fluorescence emission spectra were recorded at 550-800 nm range, after 5 min of incubation. The Stern-Volmer quenching constant (K_{SV}) values were calculated according to the decay of the emission bands of EB-DNA using Equation 4 through a plot of F_0/F *versus* [DNA]:

$$\frac{F_0}{F} = 1 + k_q \tau_0 [Q] = 1 + K_{SV}[Q] \tag{4}$$

where F and F_0 are the fluorescence intensities in the presence and absence of a quencher, respectively. K_{SV}, k_q, τ_0 and [Q] denote Stern–Volmer quenching constant, bimolecular quenching rate constant, fluorescence lifetime for EB-DNA adducts (23 ns)[14] and the concentration of quencher, respectively. According to Equation 4, the K_{SV} values were calculated from the slope and k_q is equal K_{SV}/τ_0.

In order to quantify the displacement ability of the derivatives under study, it was used minimum ligand concentration that decreases in about 50% of the EB fluorescence emission (in this case, assumed to be 50% displacement of EB).[15] The values for apparent binding constant with CT-DNA (K_{app}) were calculated using Equation 5:

$$K_{EB}[EB] = K_{app}[\text{compound}] \tag{5}$$

View Article Online
DOI: 10.1039/D0NJ04530F

where K_{EB} (4.95×10^5 M^{-1}) is the DNA-binding constant of EB, [EB] is the EB concentration (1.40×10^{-6} M), and [compound] is the concentration of the derivatives used to obtain 50% reduction in fluorescence emission intensity of EB dye.

Steady-state fluorescence emission for HSA-binding assays

The experimental binding ability between human serum albumin (HSA) and compounds **7aa-ae/7ba-be** was performed by steady-state fluorescence emission measurements at room temperature in PBS buffer (pH 7.2), using DMSO stock solution of heterocycle derivatives (10^{-5} M range). As excitation and emission fluorescence wavelengths were used 290 and 300-500 nm range, respectively. In order to obtain quantitative values for albumin fluorescence quenching data (K_{SV} and k_q values), it was used the same Stern–Volmer approximation (Equation 4) described in the CT-DNA binding assays, however for HSA was used τ_0 = 5.67 ns as fluorescence lifetime.[16]

Generally, double logarithmic approximation (Equation 6) is used to estimate the Stern-Volmer binding constant (K_a) and number of binding sites (n) for the compound–HSA adduct:

$$\log\left(\frac{F_0 - F}{F}\right) = \log K_a + n\log[Q] \qquad (6)$$

where F_0 and F represent fluorescence intensities in the absence and presence of derivatives, respectively, while [Q] is the quencher concentration. According to Equation 6, the K_a values were calculated from the interception and n by the slope.

The standard Gibbs' free-energy (ΔG^o) for compound-HSA adduct was calculated from the K_a values, using Equation 3 previous described in the CT-DNA binding assays.

Molecular docking procedure

The chemical structure for the naphthylethenyl-substituted 1,3,4-oxadiazolyl-1,2,4-oxadiazoles **7aa-ae** and **7ba-be** was built and energy-minimized by Density Functional Theory (DFT) calculations, with B3LYP potential and basis set 6-31G*, available in the Spartan'18 software (Wavefunction Inc., Irvine, CA, USA).[17] The crystallographic structures of HSA and DNA were obtained from Protein Data Bank (PDB), with access code 1N5U[18] and 1BNA,[19] respectively. The molecular docking studies were performed with GOLD 5.6 software (CCDC, Cambridge Crystallographic Data Centre, CB2 1EZ, UK).[20] The hydrogen atoms were added to the

View Article Online
DOI: 10.1039/D0NJ04530F

biomacromolecules structure according to the data inferred by GOLD 5.6 software on the ionization and tautomeric states. For the albumin, molecular docking calculations were explored with a 10 Å radius around the three main binding pockets: sites I, II, and III. On the other hand, for DNA structure, a 5.0 Å radius around the major and minor grooves of the double helix was defined for the molecular docking calculations. The number of genetic operations (crossover, migration, mutation) in each docking run used in the search procedure was set to 100,000. The scoring function used was 'ChemPLP', which is the default function of the GOLD 5.6 software. The figures were generated by PyMOL Molecular Graphics System 1.0 level software (Delano Scientific LLC software San Carlos, CA, USA).[21]

Synthetic procedures

All reactants and solvents, unless noted, were commercially available (Sigma-Aldrich®, Alfa-Aesar®, Merck®, Vetec® and Synth®). Solvents were purified in accordance to standard procedures, namely by means of distillation and drying over molecular sieves, as described elsewhere. Intermediates and products were prepared as described below.

(*E*)-3-Arylprop-2-enoic acids (**2a-b**)[22]

To a round-bottom two-necked balloon, under magnetic stirring, aldehyde **1a-b** (10 mmol) and malonic acid (10 mmol) were dissolved in pyridine (10 mL), and 5 drops of piperidine was added to the mixture. The system was stirred at reflux temperature for 15 h. Then, the mixture was poured on water-ice (50 mL), and acidified with 6 M aqueous HCl until pH 2. The suspension was extracted three times with ethyl acetate (50 ml each time). The combined organic phase was dried over anhydrous magnesium sulfate, and then filtered. The solvent was removed by rotary evaporation under reduced pressure, and the product was recrystallized from dichloromethane/hexane.

View Article Online
DOI: 10.1039/D0NJ04530F

*(E)-3-Phenylprop-2-enoic acid (cinnamic acid) (**2a**)*

Yield = 0.977 g, 66% (white solid); mp = 126.7 – 130.8 °C. ^{1}H NMR ($CDCl_3$, 400 MHz), δ (ppm): 7.67 – 7.65 (m, 2 H), 7.60 (d, J = 16.0 Hz, 1 H), 7.42 – 7.39 (m, 3 H), 6.52 (d, J = 16.0 Hz, 1 H). ^{13}C NMR ($CDCl_3$, 100 MHz), δ (ppm): 167.5, 143.9, 134.2, 130.1, 128.9, 128.1, 119.2.

*(E)-3-(Naphthalen-1-yl)prop-2-enoic acid (**2b**)*

Yield = 1.188 g, 60% (yellow solid); mp = 152.7 – 156.8 °C. ^{1}H NMR ($CDCl_3$, 400 MHz), δ (ppm): 8.40 (d, J = 15.8 Hz, 1 H), 8.18 (d, J = 8.4 Hz, 1 H), 8.01 – 7.92 (m, 3 H), 7.63 – 7.52 (m, 3 H), 6.61 (d, J = 15.7 Hz, 1 H). ^{13}C NMR ($CDCl_3$, 100 MHz), δ (ppm): 167.6, 140.3, 133.4, 131.1, 130.9, 130.5, 128.8, 127.3, 126.4, 125.8, 125.3, 123.1, 122.0.

Arylamidoximes (**4a-e**)[23]

To a round- bottom two-necked balloon, under magnetic stirring, aryl nitrile **3a-e** (15 mmol) was dissolved in ethanol (25 mL) and to the solution were added hydroxylamine hydrochloride (2.085 g, 30 mmol) and aqueous NaOH (2 equiv, 10 mL). The mixture was stirred at room temperature for 15 to 24 h, monitoring the reaction by TLC. After, the solvent was removed under rotary evaporation and to the crude mixture was added water (20 mL). The mixture was extracted with ethyl acetate (3 x 20 mL) and the organic layer was dried over anhydrous $MgSO_4$ and filtered. The solvent was removed by rotary evaporation and the product was recrystallized from chloroform – hexane.

*(Z)-N'-hydroxybenzimidamide (**4a**)*

Yield = 2.000 g, 98% (white solid). ^{1}H NMR (DMSO-d_6, 400 MHz), δ (ppm): 9.52 (br, 1 H), 7.68 (ddd, J^1 = 5.5 Hz; J^2 = 3.0 Hz; J^3 = 1.5 Hz, 2 H), 7.39 – 7.35 (m, 3 H), 5.69 (br, 2 H). ^{13}C NMR (DMSO-d_6, 100 MHz) δ (ppm): 150.8, 133.3, 128.7, 127.9, 125.3.

*(Z)-N'-hydroxy-4-mehylbenzimidamide (**4b**)*

Yield = 1.395 g, 62% (white solid). ^{1}H NMR (DMSO-d_6, 400 MHz), δ (ppm): 9.46 (br, 1 H), 7.56 (d, J = 8.0 Hz, 2 H), 7,17 (d, J = 7.8 Hz, 2 H), 5.64 (br, 2 H), 2.30

View Article Online
DOI: 10.1039/D0NJ04530F

(s, 3 H). ^{13}C NMR (DMSO-d_6, 100 MHz) δ (ppm): 150.9, 138.3, 130.5, 128.6, 125.3, 20.7.

*(Z)-N'-hydroxy-4-methoxybenzimidamide (**4c**)*

Yield = 2.116 g, 85% (grey-white solid). ^{1}H NMR (DMSO-d_6, 400 MHz), δ (ppm): 9,41 (br, 1 H), 7,61 (d, J = 8.9 Hz, 2 H), 6.92 (d, J = 8.9 Hz, 2 H), 5.66 (br, 2 H), 3.77 (s, 3 H). ^{13}C NMR (DMSO-d_6, 100 MHz) δ (ppm): 159.8, 150.7, 126.7, 125.7, 113.4, 55.1.

*(Z)-N'-hydroxy-4-chlorobenzimidamide (**4d**)*

Yield = 2.532 g, > 95% (white solid). ^{1}H NMR (DMSO-d_6, 400 MHz), δ (ppm): 9.68 (s, 1 H), 7.69 (d, J = 7.7 Hz, 2 H), 7.42 (d, J = 8.9 Hz, 2 H), 5.80 (br, 2H). ^{13}C NMR (DMSO-d_6, 100 MHz) δ (ppm): 150.0, 133.5, 132.2, 128.1, 127.1.

*(Z)-N'-hydroxy-4-trifluoromethylbenzimidamide (**4e**)*

Yield = 3.029 g, > 95% (white solid). ^{1}H NMR (DMSO-d_6, 400 MHz), δ (ppm): 9.88 (s, 1 H), 7.90 (d, J = 8.0 Hz, 2 H), 7.72 (d, J = 8.2 Hz, 2 H), 5.92 (br, 2 H). ^{13}C NMR (DMSO-d_6, 100 MHz) δ (ppm): 149.9, 137.3, 129.1 (q, J = 31.7 Hz); 126.1, 124.9 (q, J = 3.8 Hz); 124.2 (q, J = 272.2 Hz).

Ethyl 3-aryl-1,2,4-oxadiazole-5-carboxylates **(5a-e)**[24]

To a round-bottom two-necked balloon mounted with a reflux condenser, provided with magnetic stirring, a proper amidoxime **4a-e** (10 mmol) was dissolved in tetrahydrofuran (20 mL). Thereafter, *N*,*N'*-diisopropylethylamine (2.6 mL, 15 mmol) was added and the system was cooled to 0 – 5 °C. Then, ethyl oxalyl chloride (1.3 mL, 12 mmol) was added dropwise under stirring; the reaction was warmed to room temperature and kept under reflux for 2 h. After completion, the reaction mixture was cooled to room temperature, aqueous 2 N HCl solution (10 mL) and water (100 mL) were added and the product was extracted with ethyl acetate (3 x 25 mL). The organic layer was washed with aqueous $NaHCO_3$ and then with water. The organic layer was dried over anhydrous $MgSO_4$, filtered and the solvent removed by rotary evaporation. The crude product was purified through flash column chromatography on silica gel, using hexanes: ethyl acetate (85:15 v/v) and dried under reduced pressure.

View Article Online
DOI: 10.1039/D0NJ04530F

*Ethyl 3-phenyl-1,2,4-oxadiazole-5-carboxylate (**5a**)*

Yield = 1.809 g, 83% (white solid). ^{1}H NMR ($CDCl_3$, 400 MHz), δ (ppm): 8.15 (d, 2 H, J = 6.6 Hz), 7.56 – 7.47 (m, 3 H), 4.57 (q, J = 7.1 Hz, 2 H), 1.49 (t, J = 7.1 Hz, 3 H). ^{13}C NMR ($CDCl_3$, 100 MHz) δ (ppm): 169.5, 166,7, 154.3, 131.8, 129.0, 127.8, 125.8, 63.9, 14.1.

*Ethyl 3-(4-methylphenyl)-1,2,4-oxadiazole-5-carboxylate (**5b**)*

Yield = 1.694 g, 73% (white solid). ^{1}H NMR ($CDCl_3$, 400 MHz), δ (ppm): 8.03 (d, J = 8.2 Hz, 2 H), 7.29 (d, J = 8.0 Hz, 2 H), 4.56 (q, J = 7.2 Hz, 2 H), 2.41 (s, 3 H), 1.48 (t, J = 7.2 Hz, 3 H). ^{13}C NMR ($CDCl_3$, 100 MHz) δ (ppm): 169.5, 166.5, 154.2, 142.3, 129.7, 127.6, 122.9, 63.8, 21.5, 14.0.

*Ethyl 3-(4-methoxyphenyl)-1,2,4-oxadiazole-5-carboxylate (**5c**)*

Yield = 1.835 g, 74% (white solid). ^{1}H NMR ($CDCl_3$, 400 MHz), δ (ppm): 8.07 (d, J = 9.0 Hz, 2 H), 6.99 (d, J = 9.0 Hz, 2H), 4.56 (q, J = 7.1 Hz, 2 H), 3.87 (s, 3 H), 1.48 (t, J = 7.1 Hz, 3 H). ^{13}C NMR ($CDCl_3$, 100 MHz) δ (ppm): 169.2, 166.4, 162.5, 154.3, 129.4, 118.1, 114.4, 63.8, 55.4, 14.0.

*Ethyl 3-(4-chlorophenyl)-1,2,4-oxadiazole-5-carboxylate (**5d**)*

Yield = 2.146 g, 85% (white solid). ^{1}H NMR ($CDCl_3$, 400 MHz), δ (ppm): 8.08 (d, J = 8.7, 2 H), 7.48 (d, J = 8.7 Hz, 2 H), 4.57 (q, J = 7.2 Hz, 2 H), 1.49 (t, J = 7.2 Hz, 3 H). ^{13}C NMR ($CDCl_3$, 100 MHz) δ (ppm): 168.7, 166.8, 154.0, 138.1, 129.34; 129.0, 124.2, 63.9, 14.0.

*Ethyl 3-(4-trifluoromethylphenyl)-1,2,4-oxadiazole-5-carboxylate (**5e**)*

Yield = 2.460 g, 86% (white solid). ^{1}H NMR ($CDCl_3$, 400 MHz), δ (ppm): 8.28 (d, J = 8.0 Hz, 2 H), 7.77 (d, J = 8.1 Hz, 2 H), 4.59 (q, J = 7.1 Hz, 2 H), 1.50 (t, J = 7.1 Hz, 3 H). ^{13}C NMR ($CDCl_3$, 100 MHz) δ (ppm): 168.4, 167.1, 153.9, 133.6 (q, J = 32.8 Hz), 129.1, 128.1, 126.0 (q, J = 3.7 Hz), 123.6 (q, J = 272.8 Hz), 64.0, 13.9.

View Article Online
DOI: 10.1039/D0NJ04530F

3-Aryl-1,2,4-oxadiazole-5-carbohydrazides **(6a-e)**[25]

In a round-bottom flask, ethyl 3-aryl-1,2,4-oxadiazole-5-carboxylate **5a-e** (6 mmol) was dissolved in ethanol (15 mL) under magnetic stirring. Then, hydrazine hydrate (0.6 mL, 12 mmol) was added and a precipitate of the hydrazide readily formed. The mixture was kept under stirring at room temperature for 1 h, after which the precipitated hydrazide was collected by vacuum filtration and washed with cold ethanol (50 mL). The solid was transferred to another balloon and was dried under reduced pressure.

*3-Phenyl-1,2,4-oxadiazole-5-carbohydrazide (**6a**)*

Yield =1.222 g, > 95% (white solid). ^{1}H NMR (DMSO-d_6, 400 MHz), δ (ppm): 10.66 (br, 1 H), 8.05 (d, J = 7.9 Hz, 2 H), 7.65 – 7.57 (m, 3 H), 4.99 (br, 2 H). ^{13}C NMR (DMSO-d_6, 100 MHz) δ (ppm): 169.0, 167.9, 151.7, 131.8, 129.2, 127.0, 125.4.

*3-(4-Methylphenyl)-1,2,4-oxadiazole-5-carbohydrazide (**6b**)*

Yield = 1.086 g, 83% (white solid). ^{1}H NMR (DMSO-d_6, 400 MHz), δ (ppm): 7.92 (d, J = 8.2 Hz, 2 H), 7.38 (d, J = 7.9 Hz, 2 H), 2.38 (s, 3 H). ^{13}C NMR (DMSO-d_6, 100 MHz) δ (ppm): 168.9, 167.9, 151.8, 141.9, 129.8, 127.1, 122.7, 21.0.

3-(4-Methoxyphenyl)-1,2,4-oxadiazole-5-carbohydrazide (***6c***)

Yield = 1.264 g, 90% (white solid). ^{1}H NMR (DMSO-d_6, 400 MHz), δ (ppm): 7.98 (d, J = 9.0 Hz, 2 H), 7.13 (d, J = 9.0 Hz, 2 H), 3.84 (s, 3 H). ^{13}C NMR (DMSO-d_6, 100 MHz) δ (ppm): 168.8, 167.7, 162.0, 157.8, 151.8, 128.9, 117.8, 114.8, 55.4.

*3-(4-Chlorophenyl)-1,2,4-oxadiazole-5-carbohydrazide (**6d**)*

Yield =1.428 g, > 95% (white solid). ^{1}H NMR (DMSO-d_6, 400 MHz), δ (ppm): 10.78 (br, 1 H), 8.04 (d, J = 8.7 Hz, 2 H); 7.66 (d, J = 8.7 Hz, 2 H), 4.95 (br, 2 H). ^{13}C NMR (DMSO-d_6, 100 MHz) δ (ppm): 169.2, 167.2, 151.6, 136.7, 129.5, 128.9, 124.4.

*3-(4-trifluoromethylphenyl)-1,2,4-oxadiazole-5-carbohydrazide (**6e**)*

Yield = 1.306 g, 80% (white solid). ^{1}H NMR (DMSO-d_6, 400 MHz), δ (ppm): 10.84 (br, 1 H), 8.24 (d, J = 8.1 Hz, 2 H), 7.96 (d, J = 8.1 Hz, 2 H), 5.03 (br, 2H). ^{13}C

View Article Online
DOI: 10.1039/D0NJ04530F

NMR (DMSO-d_6, 100 MHz) δ (ppm): 169.5, 167.0, 151.6, 131.7 (q, J = 32.1 Hz), 129.4, 128.0, 126.3 (q, J = 3.6 Hz), 123.7 (q, J = 272.7 Hz).

(*E*)-3-Aryl-5-(5-(2-arylethen-1-yl)-1,3,4-oxadiazol-2-yl)-1,2,4-oxadiazoles (7aa-be)[9,26]

To a round-bottom, two-necked balloon, carboxylic acid **2a-b** (0.5 mmol) and a proper hydrazide **6a-e** (0.5 mmol) were suspended in dichloromethane (7.0 mL), and triethylamine (5 equiv.) was added. Then, TBTU (1.1 equiv.) was added, and the mixture was stirred at room temperature for 2 h. After completion, as verified by TLC, 4-toluenesulfonyl chloride (3 equiv.) was added to the reaction vessel and the mixture was stirred at room temperature for 2 h. The reaction was quenched using 5.0 mL of aqueous 35% ammonia solution, and stirring was continued for additional 15 min. Dichloromethane (20 mL) was added and the organic phase was transferred to an Erlenmeyer flask, and then it was dried over anhydrous magnesium sulphate. The resulting phase was filtered and solvent was removed by rotary evaporation under reduced pressure. The crude product was purified through flash chromatography employing hexanes/ ethyl acetate/ dichloromethane (7:2:1, v/v) mixture, and the solvent was removed under reduced pressure.

*(E)-3-phenyl-5-(5-(2-phenylethen-1-yl)-1,3,4-oxadiazol-2-yl)-1,2,4-oxadiazole (**7aa**)*

Yield = 0.114 g, 72% (white solid). mp = 151.8 – 153.8 °C. ^{1}H NMR ($CDCl_3$, 400 MHz), δ (ppm): 8.20 (d, J = 8.1 Hz, 2 H), 7.85 (d, J = 16.5 Hz, 1 H), 7.63 – 7.60 (m, 2 H), 7.57 – 7.51 (m, 3 H), 7.47 – 7.44 (m, 3 H), 7.13 (d, J = 16.5 Hz, 1 H). ^{13}C NMR ($CDCl_3$, 100 MHz) δ (ppm): 169.5, 166.2, 162.8, 152.6, 142.5, 134.1, 132.0, 130.8, 129.1, 129.0, 127.9, 127.7, 125.4, 108.3. HRMS-ESI(+) *m/z*, calcd. for $C_{18}H_{13}N_4O_2$ $[M + H]^+$: 317.1039; found: 317.1026.

*(E)-3-(4-methylphenyl)-5-(5-(2-phenylethen-1-yl)-1,3,4-oxadiazol-2-yl)-1,2,4-oxadiazole (**7ab**)*

Yield = 0.134 g, 81% (white solid); mp = 169.9 – 171.4 °C. ^{1}H NMR ($CDCl_3$, 400 MHz), δ (ppm): 8.08 (d, J = 8.2 Hz, 2 H), 7.84 (d, J = 16.5 Hz, 1 H), 7.62 – 7.59 (m, 2 H), 7.47 – 7.42 (m, 3 H), 7.32 (d, J = 7.9 Hz, 2 H), 7.12 (d, J = 16.4 Hz, 1 H),

View Article Online
DOI: 10.1039/D0NJ04530F

2.43 (s, 3H). ^{13}C NMR ($CDCl_3$, 100 MHz) δ (ppm): 169.6, 166.2, 162.6, 152.7, 142.5, 142.5, 134.2, 130.8, 129.7, 129.1, 127.9, 127.7, 122.7, 108.4, 21.6. HRMS-ESI(+) *m/z*, calcd. for $C_{19}H_{15}N_4O_2$ $[M + H]^+$: 331.1195; found: 331.1197.

*(E)-3-(4-methoxyphenyl)-5-(5-(2-phenylethen-1-yl)-1,3,4-oxadiazol-2-yl)-1,2,4-oxadiazole (**7ac**)*

Yield = 0.151 g, 87% (white solid); mp = 163.7 – 166.0 °C. ^{1}H NMR ($CDCl_3$, 400 MHz), δ (ppm): 8.12 (d, *J* = 8.9 Hz, 2 H), 7.83 (d, *J* = 16.5 Hz, 1 H), 7.62 – 7.59 (m, 2 H), 7.47 – 7.42 (m, 3 H), 7.12 (d, *J* = 16.5 Hz, 1 H), 7.01 (d, *J* = 8.9 Hz, 2 H), 3.87 (s, 3 H). ^{13}C NMR ($CDCl_3$, 100 MHz) δ (ppm): 169.2, 166.2, 162.6, 162.5, 152.7, 142.4, 134.1, 130.8, 129.4, 129.1, 127.9, 117.8, 114.5, 108.4, 55.4. HRMS-ESI(+) *m/z*, calcd. for $C_{19}H_{15}N_4O_3$ $[M + H]^+$: 347.1144; found: 347.1142.

*(E)-3-(4-chlorophenyl)-5-(5-(2-phenylethen-1-yl)-1,3,4-oxadiazol-2-yl)-1,2,4-oxadiazole (**7ad**)*

Yield = 0.130 g, 74% (white solid), mp = 176.7 – 179.2 °C**.** ^{1}H NMR ($CDCl_3$, 400 MHz), δ (ppm): 8.14 (d, *J* = 8.8 Hz, 2 H), 7.85 (d, *J* = 16.5 Hz, 1 H), 7.62 – 7.59 (m, 2 H), 7.51 (d, *J* = 8.8 Hz, 2 H), 7.48 – 7.43 (m, 3 H), 7.13 (d, *J* = 16.5 Hz, 1 H). ^{13}C NMR ($CDCl_3$, 100 MHz) δ (ppm): 168.8, 166.3, 163.0, 152.5, 142.7, 138.4, 134.1, 130.9, 129.4, 129.2, 129.1, 127.9, 124.0, 108.3. HRMS-ESI(+) *m/z*, calcd. for $C_{18}H_{12}ClN_4O_2$ $[M + H]^+$: 351.0649; found: 351.0645.

*(E)-3-(4-(trifluoromethyl)phenyl)-5-(5-(2-phenylethen-1-yl)-1,3,4-oxadiazol-2-yl)-1,2,4-oxadiazole (**7ae**)*

Yield = 0.086 g, 45% (white solid), mp = 192.0 – 195.3 °C. ^{1}H NMR ($CDCl_3$, 400 MHz), δ (ppm): 8.33 (d, *J* = 8.1 Hz, 2 H), 7.86 (d, *J* = 16.5 Hz, 1 H), 7.80 (d, *J* = 8.2 Hz, 2 H), 7.65 – 7.57 (m, 2 H), 7.49 – 7.41 (m, 3H), 7.14 (d, *J* = 16.5 Hz, 1 H). ^{13}C NMR ($CDCl_3$, 100 MHz) δ (ppm): 168.6, 166.4, 163.3, 152.5, 142.8, 134.2, 133.8 (q, *J* = 32.9 Hz), 130.9, 129.2, 128.9, 128.2, 128.0, 126.1 (q, *J* = 3.7 Hz), 123.6 (q, *J* = 272.5 Hz), 108.3. HRMS-ESI(+) *m/z*, calcd. for $C_{19}H_{12}F_3N_4O_2$ $[M + H]^+$: 385.0912; found: 385.0908.

View Article Online
DOI: 10.1039/D0NJ04530F

*(E)-3-phenyl-5-(5-(2-(naphthalen-1-yl)ethen-1-yl)-1,3,4-oxadiazol-2-yl)-1,2,4-oxadiazole (**7ba**)*

Yield = 0.101 g, 55% (yellow solid); mp = 155.8 – 159.8 °C. ^{1}H NMR ($CDCl_3$, 400 MHz), δ (ppm): 8.64 (d, J = 16.2 Hz, 1 H), 8.25 – 8.20 (m, 3 H), 7.93 (d, J = 8.2 Hz, 1 H), 7.89 (d, J = 8.2 Hz, 1 H), 7.85 (d, J = 7.2 Hz, 1 H), 7.63 (t, J = 7.7 Hz, 1 H), 7.57 – 7.51 (m, 5 H), 7.21 (d, J = 16.2 Hz, 1 H). ^{13}C NMR ($CDCl_3$, 100 MHz) δ (ppm): 169.6, 166.2, 162.8, 152.6, 139.4, 133.8, 132.0, 131.3, 131.2, 129.7, 129.0, 128.9, 127.8, 127.8, 127.2, 126.4, 125.5, 125.0, 123.0, 110.7. HRMS-ESI(+) *m/z*, calcd. for $C_{22}H_{15}N_4O_2$ $[M + H]^+$: 367.1195; found: 367.1195.

*(E)-3-(4-methylphenyl)-5-(5-(2-(naphthalen-1-yl)ethen-1-yl)-1,3,4-oxadiazol-2-yl)-1,2,4-oxadiazole (**7bb**)*

Yield = 0.114 g, 60% (yellow solid); m. p. = 135.4 – 139.1 °C. ^{1}H NMR ($CDCl_3$, 400 MHz), δ (ppm): 8.64 (d, J = 16.2 Hz, 1 H), 8.24 (d, J = 8.4 Hz, 1 H), 8.09 (d, J = 8.2 Hz, 2 H), 7.93 (d, J = 8.2 Hz, 1 H), 7.89 (d, J = 8.4 Hz, 1 H), 7.85 (d, J = 7.3 Hz, 1 H), 7.62 (t, J = 7.6 Hz, 1 H), 7.57 – 7.51 (m, 2 H), 7.33 (d, J = 8.0 Hz, 2 H), 7.20 (d, J = 16.2 Hz, 1 H), 2.43 (s, 3 H). ^{13}C NMR ($CDCl_3$, 100 MHz) δ (ppm): 169.6, 166.2, 162.6, 152.7, 142.5, 139.3, 133.8, 131.4, 131.3, 131.2, 129.8, 128.9, 127.7, 127.2, 126.5, 125.5, 125.0, 123.1, 122.7, 110.8, 21.6. HRMS-ESI(+) *m/z*, calcd. for $C_{23}H_{17}N_4O_2$ $[M + H]^+$: 381.1352; found: 381.1364.

*(E)-3-(4-methoxyphenyl)-5-(5-(2-(naphthalen-1-yl)ethen-1-yl)-1,3,4-oxadiazol-2-yl)-1,2,4-oxadiazole (**7bc**)*

Yield = 0.139 g, 70% (yellow solid); m. p. = 162.7 – 166.0 °C. ^{1}H NMR ($CDCl_3$, 400 MHz), δ (ppm): 8.65 (d, J = 16.2 Hz, 1 H), 8.25 (d, J = 8.5 Hz, 1 H),), 8.15 (d, J = 9.0 Hz, 2 H), 7.94 (d, J = 8.1 Hz, 1 H), 7.90 (d, J = 7.7 Hz, 1 H), 7.86 (d, J = 7.3 Hz, 1 H), 7.63 (t, J = 7.6 Hz, 1 H), 7.58 – 7.52 (m, 2 H), 7.22 (d, J = 16.2 Hz, 1 H), 7.03 (d, J = 9.0 Hz, 2 H), 3.88 (s, 3 H). ^{13}C NMR ($CDCl_3$, 100 MHz) δ (ppm): 169.3, 166.2, 162.6, 162.5, 152.8, 139.4, 133.8, 131.5, 131.3, 131.2, 129.5, 128.9, 127.2, 126.5, 125.5, 125.0, 123.1, 117.9, 114.5, 110.8, 55.4. HRMS-ESI(+) *m/z*, calcd. for $C_{23}H_{17}N_4O_3$ $[M + H]^+$: 397.1301; found: 397.1305.

View Article Online
DOI: 10.1039/D0NJ04530F

*(E)-3-(4-chlorophenyl)-5-(5-(2-(naphthalen-1-yl)ethen-1-yl)-1,3,4-oxadiazol-2-yl)-1,2,4-oxadiazole (**7bd**)*

Yield = 0.118 g, 59% (yellow solid); m. p. = 179.4 – 181.6 °C. ^{1}H NMR ($CDCl_3$, 400 MHz), δ (ppm): 8.66 (d, J = 16.2 Hz, 1 H), 8.25 (d, J = 8.5 Hz, 1 H), 8.16 (d, J = 8.8 Hz, 2 H), 7.96 (d, J = 8.2 Hz, 1 H), 7.91 (d, J = 8.1 Hz, 1 H), 7.87 (d, J = 7.2 Hz, 1 H), 7.64 (t, J = 8.4 Hz, 1 H), 7.59 – 7.55 (m, 2 H), 7.52 (d, J = 8.8 Hz, 2 H), 7.23 (d, J = 16.2 Hz, 1 H). ^{13}C NMR ($CDCl_3$, 100 MHz) δ (ppm): 168.8, 166.3, 162.9, 152.5, 139.5, 138.3, 133.8, 131.3, 131.2, 131.2, 129.4, 129.0, 128.9, 127.2, 126.5, 125.5, 125.0, 123.8, 123.0, 110.5. HRMS-ESI(+) *m/z*, calcd. for $C_{22}H_{14}ClN_4O_2$ $[M + H]^+$: 401.0805; found: 401.0790.

*(E)-3-(4-(trifluoromethyl)phenyl)-5-(5-(2-(naphthalen-1-yl)ethen-1-yl)-1,3,4-oxadiazol-2-yl)-1,2,4-oxadiazole (**7be**)*

Yield = 0.085 g, 39% (yellow solid); m. p. = 203.2 – 206.4 °C. ^{1}H NMR ($CDCl_3$, 400 MHz), δ (ppm): 8.72 (d, J = 16.2 Hz, 1 H), 8.38 (d, J = 8.1 Hz, 2 H), 8.27 (d, J = 8.5 Hz, 1 H), 7.98 (d, J = 8.2 Hz, 1 H), 7.93 (d, J = 7.7 Hz, 1 H), 7.90 (d, J = 7.1 Hz, 1 H), 7.83 (d, J = 8.2 Hz, 2 H), 7.66 (t, J = 7.6 Hz, 1 H), 7.61 – 7.56 (m, 2 H), 7.27 (d, J = 16.20 Hz, 1 H). ^{13}C NMR ($CDCl_3$, 100 MHz) δ (ppm): 168.6, 166.4, 163.2, 152.5, 139.7, 133.8, 133.6, 131.4, 131.3, 131.2, 129.0, 128.8, 128.2, 127.3, 126.5, 126.1 (q, J = 3.3 Hz), 125.6, 125.1, 123.6 (q, J = 273.4 Hz), 123.0, 110.6. HRMS-ESI(+) *m/z*, calcd. for $C_{23}H_{14}F_3N_4O_2$ $[M + H]^+$: 435.1069; found: 435.1053.

Results and Discussions

Synthesis of the target compounds

The obtention of the target compounds **7aa-be** followed the method previously adapted by our group,[9] from Stabile et al (2010),[26] which involves condensation of a carboxylic acid and a carbohydrazide, followed by cyclodehydration. Firstly, (*E*)-3-arylacrylic acids (**2a-b**) were prepared by Knoevenagel-Doebner condensation of aldehydes (**1a-b**) and malonic acid in pyridine.[22] 1,2,4-Oxadiazole-5-carbohydrazides (**6a-e**) were obtained by literature procedures, in three steps. In the first, nitriles (**3a-e**) were treated with hydroxylamine

View Article Online
DOI: 10.1039/D0NJ04530F

hydrochloride and aqueous sodium hydroxide in ethanol, giving the respective amidoximes (**4a-e**).[23] These were reacted with ethyl oxalyl chloride under basic conditions (DIPEA) in THF, forming ethyl 1,2,4-oxadiazole-5-carboxylates (**5a-e**).[24] The esters were then converted to hydrazides (**6a-e**), employing hydrazine hydrate in ethanol at room temperature.[25] (Scheme 1).

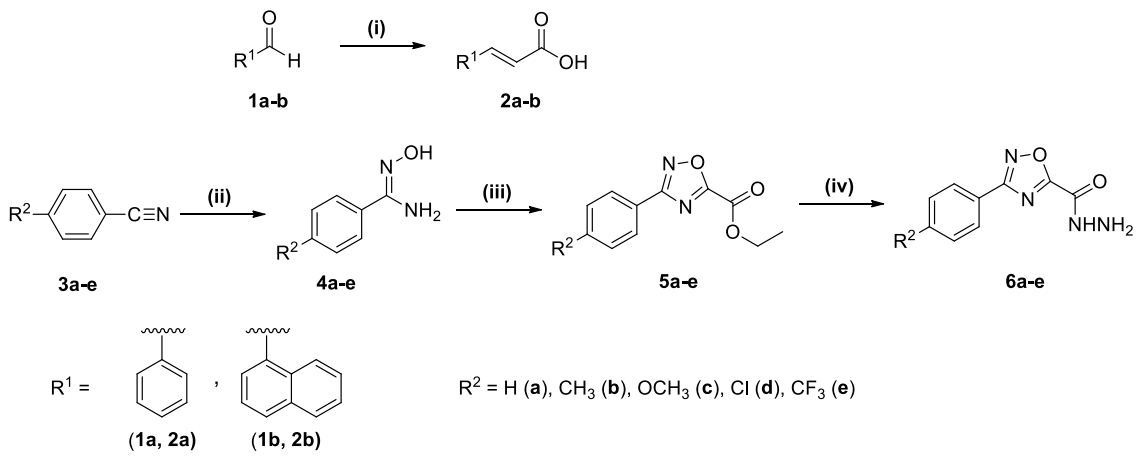

Scheme 1. Synthetic route to the acid **2** and to hydrazides **6a-e**. Conditions: i) **1a-b**, malonic acid, piperidine, pyridine, 100 °C, 15 h. ii) $NH_2OH.HCl$, EtOH, r. t., 15 h. iii) $EtO_2CC(O)Cl$, DIPEA, THF, reflux, 2h. iv) $NH_2NH_2.H_2O$, EtOH, r. t., 1 h.

Finally, the 1,3,4-oxadiazolyl-1,2,4-oxadiazoles **7aa-be** were prepared through TBTU-promoted condensation of 3-arylacrylic acids **2a-b** with the 1,2,4-oxadiazole-5-carbohydrazides **6a-e** in the presence of triethylamine, followed by cyclodehydration of the diacylhydrazine intermediates employing 4-toluenesulfonyl chloride in a one-pot procedure. A substituent series of 10 compounds was prepared for comparison. The yields of examples bearing electron-withdrawing groups were lower than those analogs bearing electron-donating groups. The results are shown in the **Table 1**.

The identity of compounds **7aa-be** was confirmed by means of ^{1}H and ^{13}C NMR spectroscopy, and High-Resolution Mass Spectroscopy (HRMS), as shown in *Synthetic Procedures* section. ^{1}H and ^{13}C spectra of compounds **7aa-be** are listed in *Supplementary Information* (Figures S1 – S20), as well as HRMS spectra (Figures S21 – S30). For X-Ray data of compound **7aa**, see *Supplementary Information* (Figure S31).

View Article Online
DOI: 10.1039/D0NJ04530F

Table 1. Substituent series of the 1,3,4-oxadiazolyl-1,2,4-oxadiazoles **7aa-be**.[a]

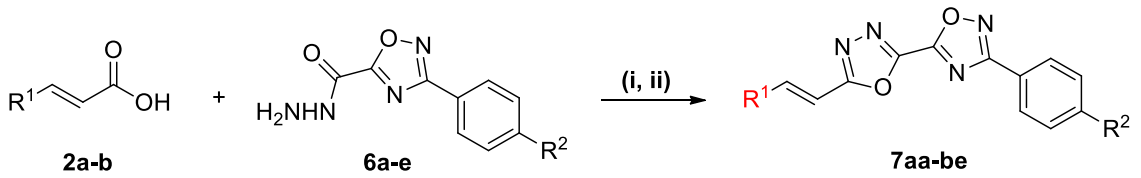

Entry	R^1	R^2	Yield (%)[b]
7aa	Ph	H	72
7ab	Ph	CH_3	81
7ac	Ph	OCH_3	87
7ad	Ph	Cl	74
7ae	Ph	CF_3	45
-	-	-	-
7ba	1-naphthyl	H	55
7bb	1-naphthyl	CH_3	60
7bc	1-naphthyl	OCH_3	70
7bd	1-naphthyl	Cl	59
7be	1-naphthyl	CF_3	39

[a]Reaction conditions: i) **2a-b** (0.5 mmol), **6a-e** (0.5 mmol), TBTU (1.1 equiv), Et_3N (5.0 equiv), DCM (7 mL), for 2 h at room temperature; ii) TsCl (3.0 equiv), 2 h at room temperature. [b]Isolated yield after column chromatography on flash silica, with hexanes/ethyl acetate/dichloromethane (7:2:1, v/v) mixture as eluent.

*UV-Vis absorption and fluorescence emission properties for derivatives **7aa-ae** and **7ba-be***

The absorption UV-Vis and steady-state fluorescence emission spectra for derivatives **7aa-ae** in $CHCl_3$ are shown in Fig. 2 and the photophysical data are listed in Table 2. All derivatives showed transition bands located at ultraviolet (UV) range, around 250-400 nm. The electronic transitions which can be related to $\pi \rightarrow \pi^*$ type-transitions are observed and no significative shift were observed when change the solvent polarity (see Table 2). The presence of a naphthyl moiety in the compounds **7ba-be** caused a significant change in the maximum absorption of the less energetic transition. This fact can be attributed to the greater contribution of aromaticity from naphthyl group. The UV-Vis spectra for the compounds **7aa-ae** in DMSO and **7ba-be** in $CHCl_3$ and DMSO are listed in the *Supplementary Information* (see Figures S32-S33).

As example, steady-state fluorescence emission spectra for the compounds **7ba-be** in argon saturated $CHCl_3$ solution are shown in Fig. 3. In general, all heterocycles contain one emission peak in the blue to cyan range (400 to 500 nm). As example, emission band shifts (~50-60 nm) can be seen when comparing the derivatives **7aa**

View Article Online
DOI: 10.1039/D0NJ04530F

(phenyl) and **7ba** (naphthyl) in the same solvent. All the compounds showed fluorescence emission with moderate quantum yields (Φ_f) in both $CHCl_3$ or DMSO solutions. The Φ_f values for these compounds also show differences; for example, compound **7ba** (naphthyl and Ph groups), compound **7bc** (naphthyl and 4-OCH_3Ph groups) and compound **7be** (naphthyl and 4-CF_3Ph groups) in $CHCl_3$ solution have distinct Φ_f values, which explains the influence of the donor/acceptor electronic properties, attributed to the resonance stabilization structures in the excited state (Table 2).

Large Stokes Shifts (SS) were observed in all derivative compounds, mainly in DMSO solution, and it can be assigned to the ICT state that exists in these structures (Table 2). Steady-state fluorescence emission spectra for compounds **7aa-ae** in $CHCl_3$ and DMSO and **7ba-be** in DMSO are listed in the *Supplementary Information* (see Figures S34-S35). The visible appearance of representative examples **7aa** and **7ba** in solution (DMSO) is shown in the *Supplementary Information* (see Figure S36).

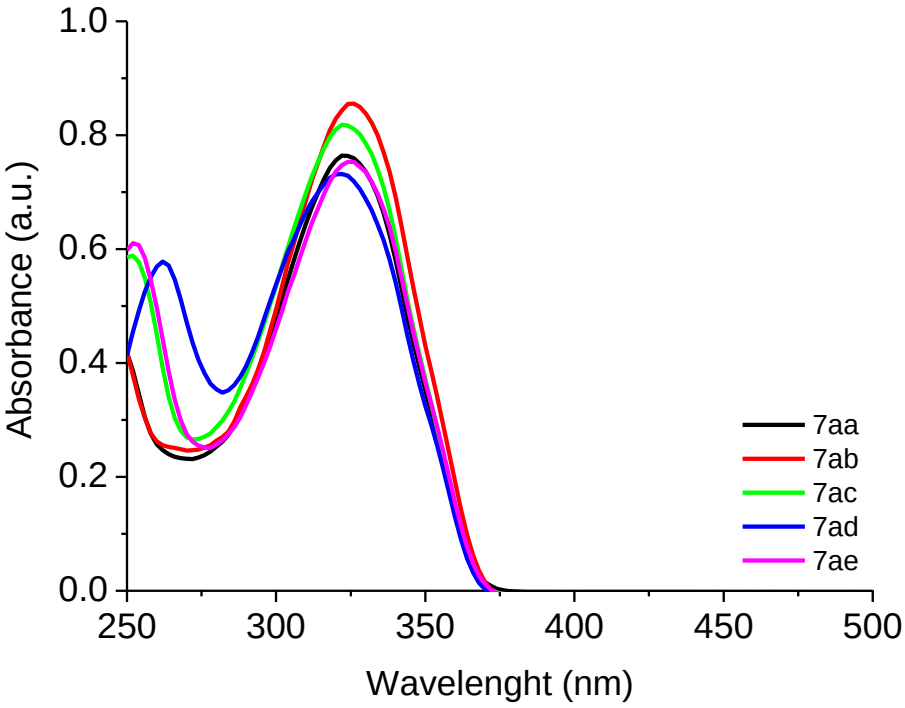

Fig. 2. UV-Vis absorption spectra of derivatives **7aa-ae** in $CHCl_3$ solution ([ ] = 2.00 x 10^{-5} M).

View Article Online
DOI: 10.1039/D0NJ04530F

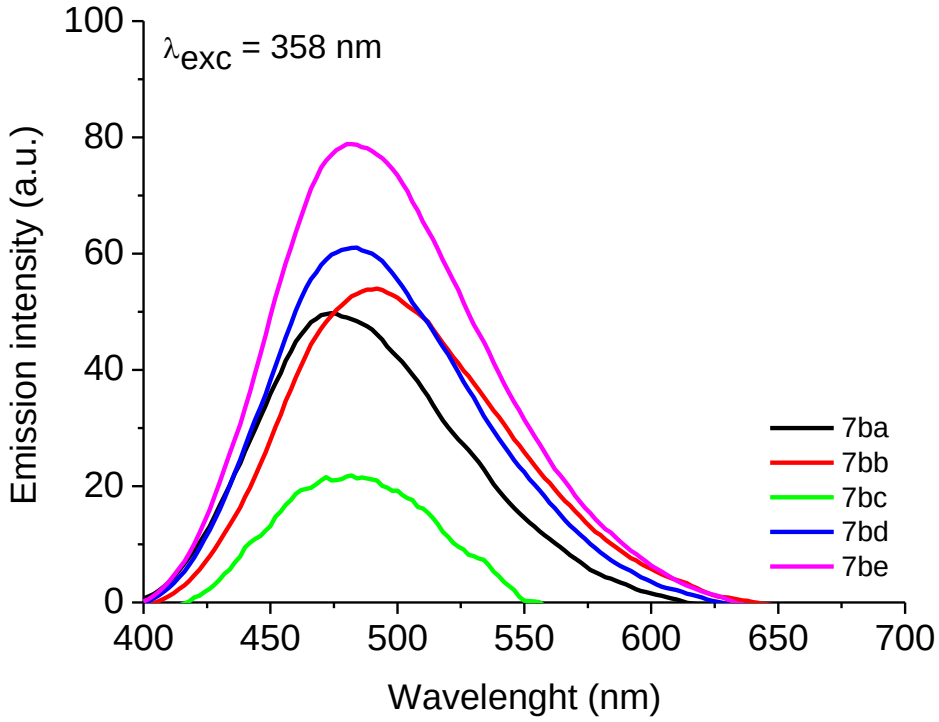

Fig. 3. Steady-state emission spectra of derivatives **7ba-be** (λ_{exc} = 358 nm) in saturated argon chloroform solution ([ ] = 1.00 x 10^{-6} M).

View Article Online
DOI: 10.1039/D0NJ04530F

Table 2. Photophysical data of compounds **7aa-ae** and **7ba-be**.

Compound	λ, nm (ε; $M^{-1}cm^{-1}$)[a]	Emission, nm (Φ_f)[b]	SS (nm)[c]	E_{0-0} (eV)[d]
	in $CHCl_3$			
7aa	323 (38,250)	426 (0.103)	103.0	3.48
7ab	325 (42,700)	432 (0.158)	107.0	3.44
7ac	252 (29,350), 322 (40,850)	429 (0.212)	107.0	3.48
7ad	262 (28,850), 321 (36,500)	425 (0.147)	104.0	3.55
7ae	253 (30,450), 325 (37,650)	429 (0.170)	104.0	3.46
7ba	261 (sh), 359 (38,300)	473 (0.274)	114.0	3.04
7bb	360 (43,100)	491 (0.335)	131.0	3.03
7bc	356 (40,250)	480 (0.015)	124.0	3.15
7bd	260 (52,950), 356 (36,300)	482 (0.357)	126.0	3.06
7be	359 (40,400)	481 (0.482)	122.0	3.06
	in DMSO			
Compound	**λ, nm (ε; $M^{-1}cm^{-1}$)[a]**	**Emission, nm (Φ_f)[b]**	**SS (nm)[c]**	**E_{0-0} (eV)[d]**
7aa	324 (39,050)	426 (0.097)	102.0	3.50
7ab	326 (40,350)	433 (0.154)	107.0	3.42
7ac	325 (39,600)	428 (0.199)	103.0	3.43
7ad	259 (31,100), 323 (37,550)	425 (0.134)	102.0	3.52
7ae	325 (39,750)	429 (0.168)	104.0	3.40
7ba	259 (32,150), 357 (31,800)	473 (0.300)	116.0	3.00
7bb	357 (27,700)	490 (0.348)	133.0	2.94
7bc	258 (39,400), 349 (19,250)	480 (0.142)	131.0	3.16
7bd	256 (47,250), 355 (23,950)	481 (0.377)	126.0	2.97
7be	256 (46,200), 356 (25,450)	481 (0.501)	125.0	3.00

[a][ ] = 2.00 x 10^{-5} M; [b][ ] = 10^{-6} M range at 298K, using 9,10-Diphenylanthracene (DPA) in $CHCl_3$ as standard (Φ_f = 0.65); [c]Stokes Shift equation: $\Delta\lambda = \lambda_{emisson} - \lambda_{absorption}$; [d]$E_{0-0}$ = 1240 / λ (in eV); sh = shoulder.

DNA-binding assays by absorption UV-Vis analysis

The interaction of compounds **7aa-ae** and **7ba-be** with CT-DNA model was studied by UV–Vis spectroscopy in DMSO(2%)/Tris-HCl buffer pH 7.2 mixture solution, at 250-500 nm range. All compounds interact with CT-DNA and gives an absorbance change in ultraviolet region. As example, the effect of different concentrations of DNA titration on the absorption spectra using compounds **7aa** and **7ba** are shown in Fig. 4.

In this experiment, upon increase concentration of CT-DNA (0-100 μM range) into solution of derivatives **7aa** and **7ba** reveals hypochromicity profile in the transitions around 300-360 nm. For all derivatives, was not observed any hypso or bathochromic shifts, indicating non-electrostatic interaction of the molecules and CT-DNA (Fig. 4). The decrease intensity changes of the related transition bands could be accounted by the interaction of the aromatic portion of the compounds, probably via hydrophobic forces (van der Waals, H-bonding or π-stacking) with the DNA biomolecule or the presence of an aromatic moiety in the structure by covalent interactions, as previously reported in the literature.[27]

The hypochromicity parameter (*H*%) and intrinsic binding constant (K_b) values for the compounds were calculated and summarized in Table 3. In the present study, the derivatives demonstrated strong binding forces to CT-DNA (K_b ~10^5 to 10^6 M^{-1}). These binding constant values are associated to the compound-DNA complex stability in solution, while the Gibb´s free energy indicates the spontaneity of derivative-DNA binding process (Table 3). The UV-Vis CT-DNA spectra of derivatives **7ab-ae** and **7bb-be** can be found in the *Supplementary Information* and presented a similar behavior (Figures S37-S44). Moreover, molecular docking calculations between compounds and DNA was performed, reinforcing the experimental results.

View Article Online
DOI: 10.1039/D0NJ04530F

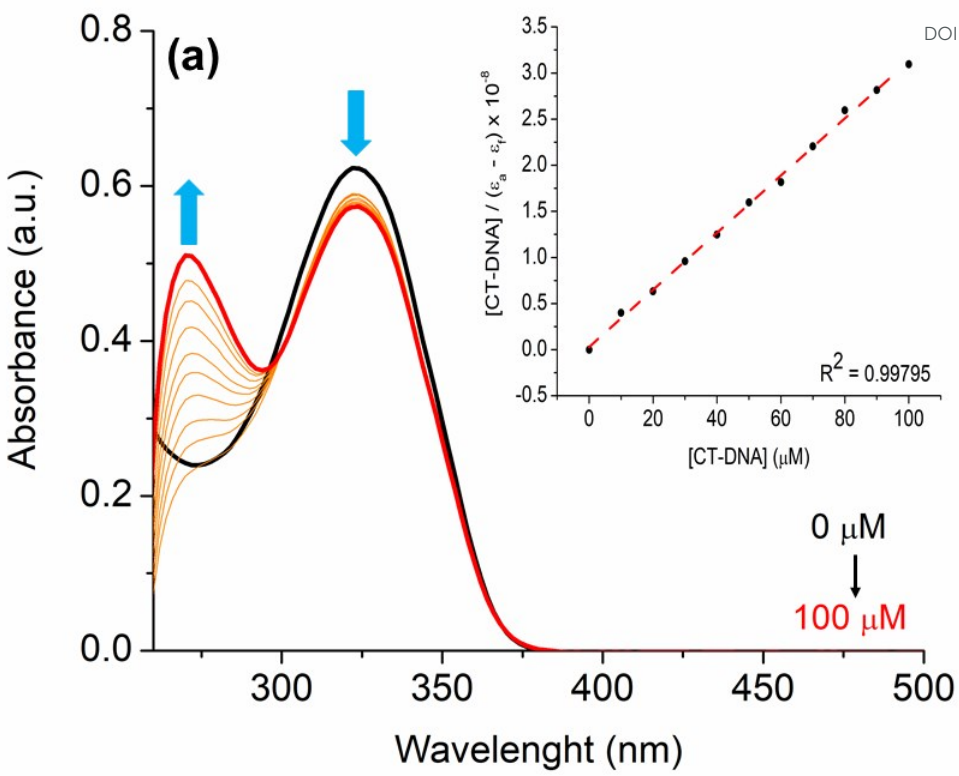

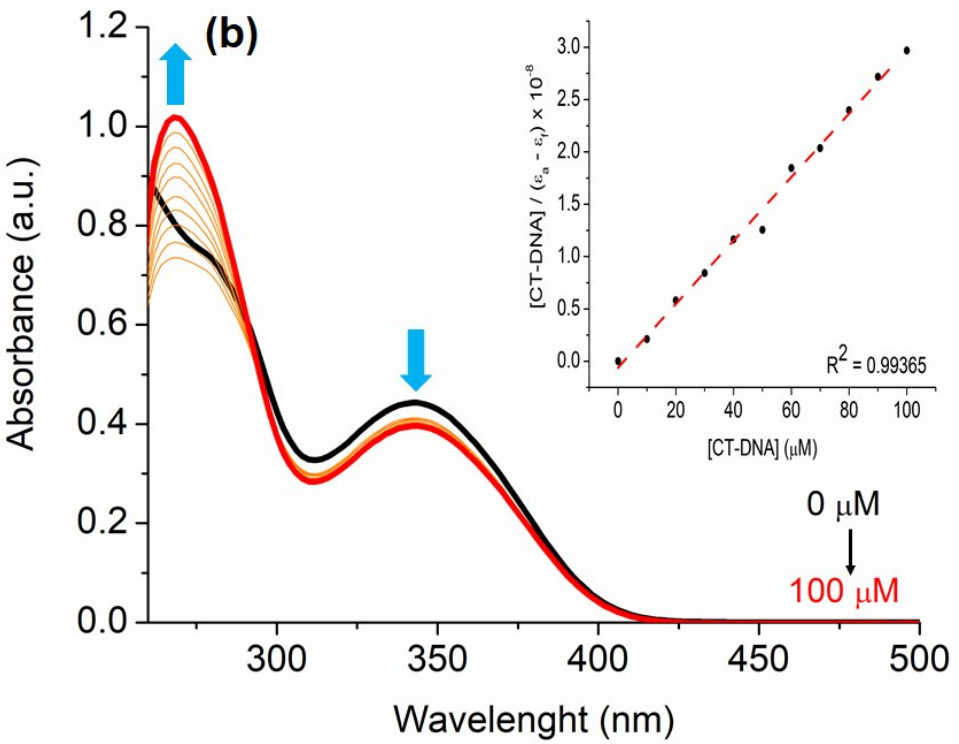

Fig. 4. UV-Vis titration absorption spectra of derivative **(a) 7aa** and **(b) 7ba**, in a DMSO (2%)/Tris-HCl buffer (pH 7.2) solution. The concentration of CT-DNA ranged from 0 to 100 μM. Insert graph shows the plot of [DNA]/($\varepsilon_a - \varepsilon_f$) *versus* [DNA].

View Article Online
DOI: 10.1039/D0NJ04530F

EB-DNA competitive assays by steady-state fluorescence emission analysis

In order to further confirm the binding affinity of the studied compounds with CT-DNA, competitive binding assays via fluorescence quenching analysis were conducted in the presence of the commercial intercalator (EB) into CT-DNA solution. Steady-state fluorescence emission analysis of fixed concentration of CT-DNA:EB adduct in the presence of derivatives **7aa** and **7ba** are shown in Figures S45-S54 in the *Supplementary Information* depict the CT-DNA:EB without and in the presence of **7ab-ae** and **7bb-be**.

The CT-DNA:EB adduct formation shows a strong fluorescence emission at λ = 645 nm when excited at λ_{exc} = 510 nm and the corresponding fluorescence intensity emission decreased upon successive addition of the compounds under study, being in accordance for some heterocyclic compounds reported in the literature.[9,27] This fact could be assigned to the competition of derivatives with the intercalator EB into CT-DNA strands. The Stern-Volmer quenching constant (K_{SV}) and bimolecular quenching rate constant (k_q) values are presented in the Table 3. In this context, the K_{SV} values suggest weak competition mode of EB-binding ($K_{SV} \sim 10^2$ M^{-1}) in the case of phenyl derivatives **7aa-ae** and good competition mode of EB-binding ($K_{SV} \sim 10^3$-10^4 M^{-1}) in the case of naphthyl derivatives **7ba-be**. Moreover, the k_q values for all derivatives indicated a probably static interaction ($k_q \sim 10^{10}$-10^{11} $M^{-1}s^{-1}$) between derivatives and CT-DNA:EB adduct (see Table 3). Again, molecular docking calculation were performed, corroborating with the experimental results.

View Article Online
DOI: 10.1039/D0NJ04530F

Table 3. Hypochromicity (*H*%), bathochromic shift (Δλ), Intrinsic binding constant (K_b), Stern-Volmer quenching constant (K_{SV}), quenching rate constant (k_q) and apparent binding constant (K_{app}) values for the interactions of compounds with calf thymus DNA (CT-DNA).

	Absorption-DNA				Emission EB-DNA			
Compound	***H*** **(%)[a]**	**Δλ (nm)[b]**	**K_b (M^{-1})[c]**	**ΔG° (kcal mol^{-1})[d]**	***Q*** **(%)[e]**	**K_{SV} (M^{-1})[f]**	**k_q ($M^{-1}s^{-1}$)[g]**	**K_{app} (M^{-1})[h]**
7aa	8.00	0.0	1.07×10^6	−8.22	10.00	7.48×10^2	3.25×10^{10}	6.44×10^5
7ab	7.70	0.0	4.07×10^6	−9.01	7.40	5.24×10^2	2.28×10^{10}	6.58×10^5
7ac	8.65	0.0	1.16×10^6	−8.27	12.10	1.26×10^3	5.48×10^{10}	6.51×10^5
7ad	8.50	0.0	6.76×10^5	−7.95	5.30	4.41×10^2	1.92×10^{10}	6.77×10^5
7ae	11.00	0.0	2.00×10^6	−8.59	8.20	9.28×10^2	4.03×10^{10}	6.70×10^5
7ba	10.80	0.0	4.94×10^5	−7.76	9.65	1.24×10^3	5.39×10^{10}	6.47×10^5
7bb	7.10	0.0	2.15×10^6	−8.63	61.40	1.69×10^4	7.34×10^{11}	4.38×10^6
7bc	11.30	0.0	1.00×10^5	−6.82	13.20	1.37×10^3	5.95×10^{10}	6.48×10^5
7bd	9.00	0.0	1.87×10^6	−8.550	57.20	1.49×10^4	6.48×10^{11}	4.48×10^6
7be	9.05	0.0	3.65×10^6	−8.945	69.00	2.50×10^4	1.08×10^{12}	3.85×10^6

[a]$H(\%) = (Abs_{initial} - Abs_{final})/(Abs_{initial}) \times 100$; [b]$\Delta\lambda$ (nm) = $\lambda_{final} - \lambda_{initial}$; [c]Intrinsic binding constant by UV-Vis CT-DNA analysis; [d]Gibb´s free energy (R = 1.987 cal mol^{-1} K^{-1} and T = 298K); [e]$Q(\%) = (Em_{initial} - Em_{final})/(Em_{initial}) \times 100$; [f]Stern-Volmer quenching EB-DNA constant (K_{SV}) by steady-state fluorescence emission spectra; [g]Bimolecular Stern-Volmer quenching rate EB-DNA constant (k_q) by steady-state fluorescence emission spectra (EB-DNA – τ_0 = 23 ns); [h]DNA-binding apparent constant (K_{app});

View Article Online
DOI: 10.1039/D0NJ04530F

HSA-binding by fluorescence quenching emission assays

HSA-binding properties can be easily determined by steady-state fluorescence emission assays through the fluorescence quenching of tryptophan (Trp) and/or tyrosine (Tyr) amino acid residues. The HSA pocket structure presents one and seventeen Trp and Tyr amino acid residues, respectively.[28] Therefore, the interaction between human serum albumin and derivatives was determined through the fluorescence quenching assays.

As example, the steady-state fluorescence emission for HSA without and in the presence of successive additions of derivatives **7aa** (ranging from 0 to 100 μM) at room temperature (298K) is shown in Fig. 5, while Figures S55-S63 in the *Supplementary information* depicts the spectra results for the other derivatives. The HSA exhibited a strong fluorescence emission peak at λ_{em} = 329 nm when excited at 290 nm. Fluorescence intensities of HSA gradually reduced upon successive additions of each compound under study, and a slightly blue shift in all cases was also observed, which suggests that **7aa-ae**/**7ba-be** interact with albumin structure, mainly with the main fluorophores present in the biomacromolecule and the shift may be explained by conformational changes and/or perturbation on the microenvironment around the albumin's fluorophores upon ligand binding.

The fluorescence quenching in a biomolecule can be induced by different mechanisms, which are in general classified into dynamic or static process. In order to evaluate the main fluorescence quenching mechanism behavior induced by the compounds **7aa-ae** and **7ba-be**, the well-known Stern–Volmer approximation was applied in this study (see *Experimental section*).

The Stern-Volmer quenching (K_{SV}) and bimolecular quenching rate (k_q) constant values for the interaction between HSA and the derivatives are shown in Table 4. In all cases, moderate K_{SV} values ($10^2 – 10^4$ M^{-1}) and high k_q values in about one/two orders of magnitude larger (e.g. $10^{11} – 10^{12}$ $M^{-1}s^{-1}$) than the diffusional collision quenching rate constant ($k_{diff} \approx 7.40 \times 10^9$ $M^{-1}s^{-1}$, according to the Smoluchowski-Stokes-Einstein theory at 298K),[29] indicate that the main fluorescence quenching mechanism is *via* static process. Therefore, there is a ground-state association between HSA:**7aa-ae** and HSA:**7ba-be**.

Since the K_a values for each compound are in the order of $10^2 – 10^3$ M^{-1} (Table 4) indicate moderate interaction ability. In addition, the number of binding sites (*n*) for all compounds are in the range of 0.70-1.90 (Table 4), suggesting the presence of one or two possible binding sites in the HSA subunits (depending on the ligand structure). Overall, the presence of different units (phenyl or naphthyl) in the organic ligands under study, cause variation in the binding constant values and there is an indication that both derivatives **7aa-ae** and **7ba-be** can be possible transported and biodistributed by serum albumin in the human bloodstream.

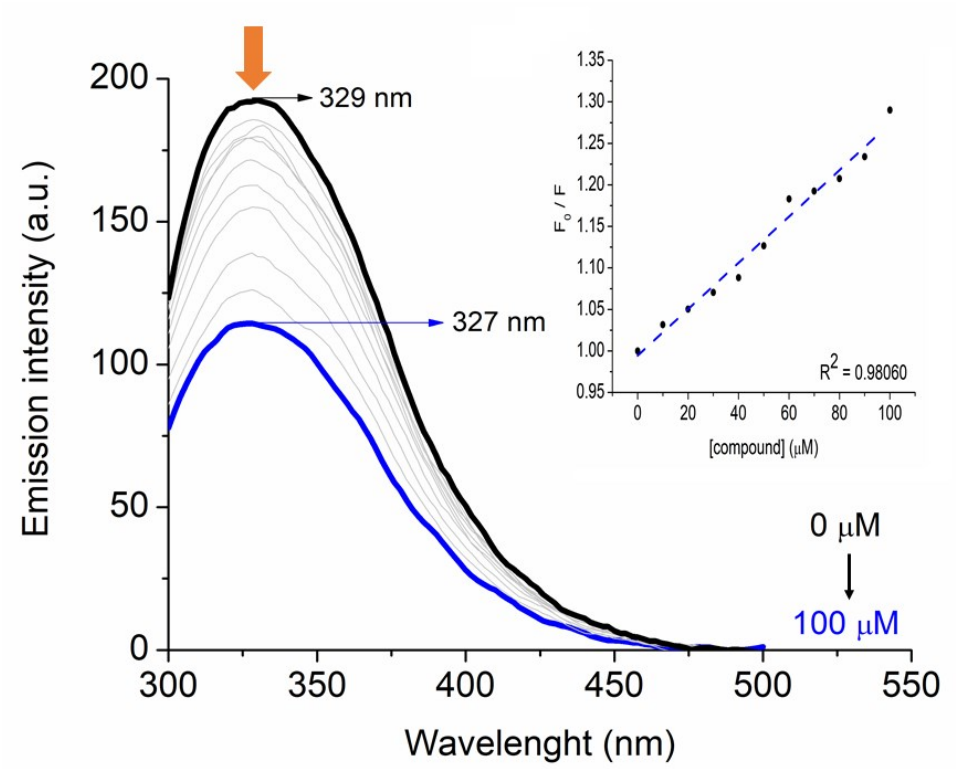

Fig. 5. HSA-binding emission spectra with derivative **7aa** in a DMSO (2%)/Tris-HCl buffer (pH 7.2) solution. The concentration of compound ranged from 0 to 100 μM. Insert graph shows the plot of F_0/F *versus* [compound].

View Article Online
DOI: 10.1039/D0NJ04530F

Table 4. HSA-binding data of derivatives **7aa-ae** and **7ba-be**.

Compound	Q (%)[a]	K_{SV} (M^{-1})[b]	k_q (M^{-1} s^{-1})[c]	K_a (M^{-1})[d]	ΔG^0 (kcal/mol)[e]	n[f]
7aa	17.80	1.55×10^3	2.73×10^{11}	1.10×10^3	−4.14	1.90
7ab	21.70	2.32×10^3	4.09×10^{11}	1.12×10^3	−4.16	1.88
7ac	19.40	1.40×10^3	2.47×10^{11}	1.24×10^3	−4.22	1.29
7ad	8.55	8.96×10^2	1.58×10^{11}	1.68×10^2	−3.03	0.70
7ae	13.75	8.20×10^2	1.44×10^{11}	2.07×10^2	−3.16	0.78
7ba	40.80	2.79×10^3	4.92×10^{11}	3.87×10^3	−4.90	1.07
7bb	51.25	9.88×10^3	1.74×10^{12}	5.20×10^3	−5.06	1.32
7bc	53.95	1.02×10^4	1.80×10^{12}	7.50×10^3	−5.28	1.86
7bd	29.50	3.86×10^3	6.80×10^{11}	3.33×10^3	−4.80	0.95
7be	28.45	3.27×10^3	5.76×10^{11}	3.96×10^3	−4.90	1.12

[a]Quenching = $(Int_{initial} - Int_{final}) / Int_{initial} \times 100$;

[b]Stern-Volmer quenching HSA constant by steady-state emission spectra;

[c]Stern-Volmer rate quenching HSA constant by steady-state emission spectra ($\tau_0 = 5.67 \times 10^{-9}$ s);

[d]Modified Stern-Volmer binding HSA constant by steady-state emission spectra;

[e]Gibb´s free-energy for HSA-molecule interaction;

[f]Number of binding sites;

Molecular docking calculations for the interaction between biomacromolecules and ***7aa-ae / 7ba-be***

Molecular docking technique is an attractive tool in drug design since it can evaluate biomacromolecule-drug interactions from an atomic point of view, gaining insights into the experimental results.[30] Thus, in order to complement the experimental data at predict the best-fit orientation of naphthylethenyl-substituted 1,3,4-oxadiazolyl-1,2,4-oxadiazoles within DNA strands and HSA, as well as identify the main intermolecular forces involved in the interaction process, molecular docking calculations were carried out.

View Article Online
DOI: 10.1039/D0NJ04530F

Table 5 shows the docking score value (dimensionless) for all synthetic compounds under study into DNA and HSA structure, respectively. For DNA, the highest docking score value was obtained in the minor groove (e.g. 71.5 and 23.2 for DNA:**7aa** in the minor and major groove, respectively), suggesting that **7aa-ae** and **7ba-be** interact preferentially in the minor groove of DNA strands (the same theoretical region for the intercalator EB presented in this work), being in accordance with previous theoretical evaluation described in the literature for EB (Table 5).[31] On the other hand, for HSA, the docking score value for the three main possible binding sites (sites I, II, and III in the subdomains IIA, IIIA, and IB, respectively) suggest that naphthylethenyl-substituted 1,3,4-oxadiazolyl-1,2,4-oxadiazoles could interact into sites II and III (not necessarily at the same time - docking score values are quite similar, Table 5), however since site II presented the highest docking score value (e.g. 62.9, 84.3, and 80.3 for HSA:**7aa** in the sites I, II, and III, respectively) all compounds bind preferentially in the subdomain IIIA. The same binding pocket in HSA was theoretically described for 1,3,4-oxadiazole derivatives of fatty acid.[32]

Fig. 6 shows the best docking pose of **7aa-e** and **7ba-be** in the minor groove of DNA. From the experimental data, the intrinsic binding constant (K_b) values for the compounds **7aa**, **7ab**, **7ac**, and **7ae** are in the same order (10^6 M^{-1}) and interesting molecular docking calculations indicated practically the same pose inside DNA strands (superposition in Fig. 6), corroborating with the experimental results. The same theoretical and experimental trend was observed for the compounds **7ba-be** (superposition in Fig. 6). Finally, Table S3 (*supplementary information*) shows the main nucleobase of DNA that interact with naphthylethenyl-substituted 1,3,4-oxadiazolyl-1,2,4-oxadiazoles, and according to the docking results van der Waals interactions are the main intermolecular forces involved in the binding process in the minor groove of DNA, also corroborating with intermolecular forces hypothesis raised in the experimental spectroscopic data.

View Article Online
DOI: 10.1039/D0NJ04530F

Table 5. Docking score value (dimensionless) for the interaction of DNA and HSA with derivatives **7aa-ae** and **7ba-be**.

	DNA		HSA		
Compound	**Minor Groove**	**Major Groove**	**Site I**	**Site II**	**Site III**
7aa	71.5	23.2	62.9	84.3	80.3
7ab	75.0	20.1	65.8	92.9	85.0
7ac	76.2	23.0	67.4	91.6	86.0
7ad	76.1	24.5	65.9	84.8	79.9
7ae	78.5	27.8	73.6	87.4	84.8
7ba	87.1	31.2	72.7	93.9	87.4
7bb	82.2	30.5	73.1	92.1	88.1
7bc	81.3	30.0	72.0	92.1	87.3
7bd	79.4	29.9	70.6	91.7	87.6
7be	85.8	30.8	76.0	90.9	90.0
EB	65.7	28.7	-	-	-

In the case of HSA studies for **7aa-ae** and **7ba-be**, molecular docking results suggested van der Waals and hydrogen bonding as the main intermolecular forces involved in the binding process into site II (Table S4 – *supplementary information*), as example the hydrogen atom from hydroxyl group of Tyr-411 and Ser-489 residues is a potential donor for hydrogen bonding with oxygen and nitrogen atoms from 1,3,4-oxadiazolyl moiety in the **7aa-ac** structures, within a distance of 2.10 and 1.90 Å, respectively, while van der Waals interactions occur for all chemical moieties of **7aa-ac** structures with Ile-388, Lys-414, Val-415, Val-433, Cys-437, Leu-453, Leu-457, Leu-460, and Phe-488 residues within a distance of 1.30, 2.80, 2.30, 3.30, 2.50, 2.40, 3.00, 2.80, 3.60, and 1.90 Å, respectively. From the experimental data for HSA, the modified Stern-Volmer binding constant (K_a) values indicated that **7aa-ac**, **7ad/ae** and **7ba-be** are in the same order of magnitude (10^3, 10^2, and 10^3 M^{-1}, respectively) and Fig. 7 shows a clear superposition of these compounds, corroborating with the spectroscopic data.

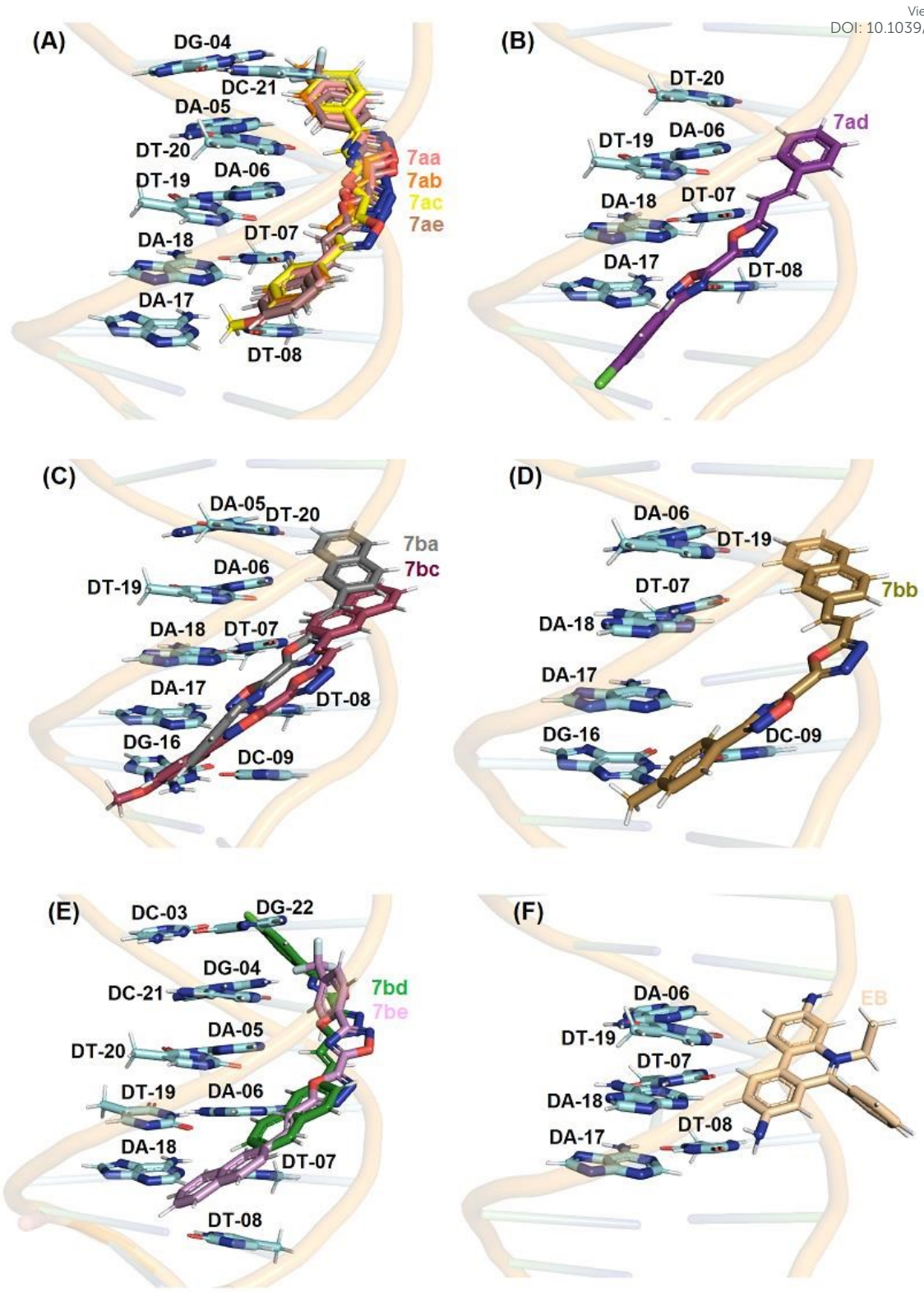

Fig. 6. Best docking pose for the interaction **(A)** DNA:**7aa-ac**/**ae**, **(B)** DNA:**7ad**, **(C)** DNA:**7ba**/**bc, (D)** DNA:**7bb**, **(E)** DNA:**7bd**/**be**, and **(F)** DNA:EB in the minor groove. Selected nucleobases are as stick representation in cyan, while **7aa-ae**, **7ba-be**, and EB structures are also as stick representation, but in different colors, according to the representation in the figure above. Elements' colors: hydrogen, nitrogen, chlorine, fluorine, and oxygen are in white, dark blue, light green, light blue, and red, respectively.

View Article Online
DOI: 10.1039/D0NJ04530F

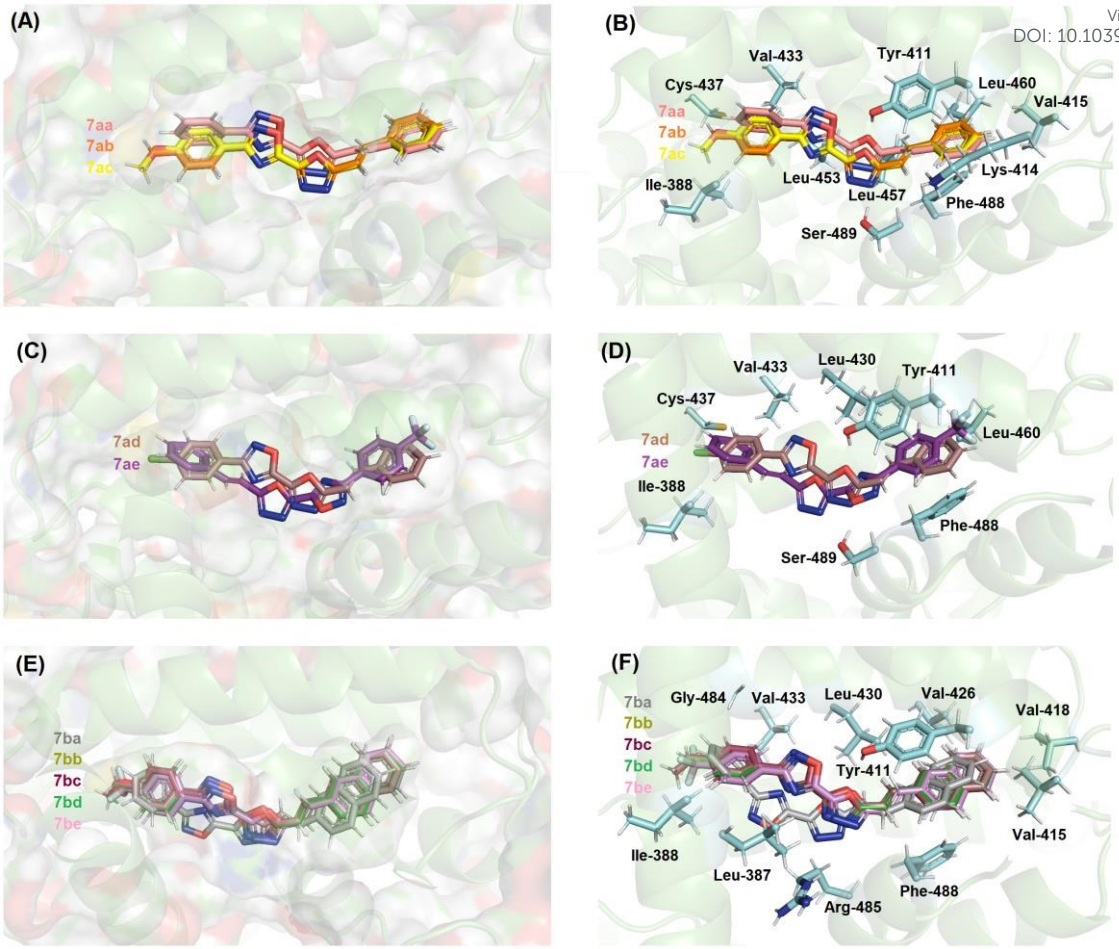

Fig. 7. (A, C, E) Protein surface for the best docking pose for **(A)** HSA:**7aa-ac**, **(C)** HSA:**7ad/ae** and **(E)** HSA:**7ba-be** in the site II (subdomain IIIA). **B**, **D** and **F**: Amino acid residues which interact with **(B) 7aa-ac**, **(C) 7ad/ae** and **(E) 7ba-be** in the site II. Selected amino acid residues are as stick representation in cyan, while **7aa-ae**, and **7ba-be** structures are also as stick representation, but in different colors, according to the representation in the figure above. Elements' colors: hydrogen, nitrogen, chlorine, fluorine, and oxygen are in white, dark blue, light green, light blue, and red, respectively.

View Article Online
DOI: 10.1039/D0NJ04530F

Conclusions

The two series of 1,3,4-oxadiazolyl-1,2,4-oxadiazole derivatives were readily accessible through the employed condensation-cyclodehydration method, despite variations in the yields, and all obtained compounds were successfully isolated and characterized. All **7aa-be** derivatives displayed observable fluorescence. When phenyl and naphthyl derivatives were analyzed through UV-Vis spectroscopy, significant differences were observed between the two series. Absorbance values, which were bathochromic for naphthyl (356 – 360 nm) when compared to phenyl derivatives (321 – 325 nm), and the large Stokes shifts observed indicate a highly conjugated structure along the molecules. The strong interaction of the compounds with CT-DNA, as elucidated by UV-Vis titration, EB displacement emission analysis and theoretical molecular docking, gave a potential target for biochemical applications, which could also be favored by the moderate interaction with the important transporter protein HSA, as verified by fluorescence-monitored titration and docking analysis. This study contributes to the understanding of 1,3,4-oxadiazolyl-1,2,4-oxadiazole as a versatile scaffold for the design of electronically conjugated molecules for physical-chemical and biochemical essays.

Conflicts of Interest

There are no conflicts of interest to declare.

Authors contribution

J.C. Mayer, L. Dornelles and B.A. Iglesias idealized the work. J.C. Mayer conducted the synthesis and characterization analysis. D.F. Back conducted the X-ray measurements. T.V. Acunha conducted the biomolecule assays. O.A. Chaves conducted the molecular docking analysis. B.A. Iglesias, J.C. Mayer and L. Dornelles wrote the manuscript.

View Article Online
DOI: 10.1039/D0NJ04530F

Supplementary data

CCDC-2027432 contain the supplementary crystallographic data for the ligand **7aa** (at the supplementary information session). These data can be obtained free of charge *via* http://www.ccdc.cam.ac.uk/conts/retrieving.html, or from the Cambridge Crystallographic Data Centre, 12 Union Road, Cambridge CB2 1EZ, UK; fax: (+44) 1223–336–033; or e–mail: deposit@ccdc.cam.ac.uk.

Acknowledgments

This research was supported by the Brazilian funding agencies: Coordenação de Aperfeiçoamento de Pessoal de Nível Superior (CAPES and CAPES/PROEX – Finance Code 001), Conselho Nacional de Desenvolvimento Científico e Tecnológico (CNPq – Universal proc. 409150/2018-5 and PG-2018 grants process 304711/2018-7).

References

1. a) Patel, D. S.; Avalani, J. R.; Raval, D. K. *J. Braz. Chem. Soc.*, **2012**, *23* (10), 1951 – 1954; b) Li, H.-J.; Zhang, Y.-Q.; Tang, L.-F. *Tetrahedron*, **2015**, *71* (40), 7681 – 7686; c) Wang, Z.; Zhang, H.; Killian, B. J.; Jabeen, F.; Pillai, G. G.; Berman, H. M.; Mathelier, M; Sibble, A. J.; Yeung, J.; Zhou, W.; Steel, P. J. *Eur. J. Org. Chem.*, **2015**, *2015* (23), 5183 – 5188.

2. a) Kayukova, L. A. *Pharm. Chem. J*, **2005**, *39* (10), 539 – 547; b) Yadav, M. R.; Shirude, S. T.; Puntambekar, D. S.; Patel, P. J.; Prajapati, H. B.; Parmar, A.; Balaraman, R.; Giridhar, R. *Acta Pharm.*, **2007**, *57* (1), 13 – 30.

3. a) Li, Z.; Zhan, P.; Liu, X. *Mini Rev. Med. Chem.*, **2011**, *11* (13), 1130 – 1142; b) Zhang, Y, Zuniga, C.; Kim, S.-J.; Cai, D.; Barlow, S.; Salman, S.; Coropceanu, V.; Brédas, J.-L.; Kippelen, B.; Marder, S. *Chem. Mater.*, **2011**, *23* (17), 4002 – 4015; c) Boström, J., Hogner, A.; Llinàs, A.; Wellner, E.; Plowright, A. T., *J. Med. Chem.*, **2012**, *55* (5), 1817 – 1830; d) Abdo, N, Y. M.; Kamel, M. M. *Chem. Pharm. Bull.* **2015**, *63* (5), 369 -376.

4. Du, K.; Cao, X.; Zhang, P.; Zheng, H. *Bioorg. Med. Chem. Lett.*, **2014**, *24* (12), 5318 – 5320.

5. Cullen, M. D.; Deng, B.-L.; Hartman, T. L.; Watson, K. M.; Buckheit, R. W.; Pannecouque, C.; De Clercq, E.; Cushman, M. *J. Med. Chem.*, **2007**, *50* (20), 4854 – 4867.

6. Tantray, M. A.; Khan, I.; Hamid, H.; Alam, M. S.; Dhulap, A.; Kalam, A. *RSC Adv.*, **2016**, *6* (49), 43345 – 43355.

7. a) Frazer, A. H.; Sweeny, W.; Wallenberger, F. T. *J. Polym. Sci. Part A: General Papers Banner*, **1964**, *2* (3), 1157 – 1169; b) Agneeswari, R.; Tamilavan, V.; Song, M.;

Kang, J.-W.; Jin, S.-H.; Hyun, M. H. *J. Polym. Sci. Part A: Polym. Chem.* **2013**, *51* (10), 2131 – 2141; c) Ganesh, S. D.; Pai, V. K.; Kariduraganavar, M. Y.; Jayanna, M. B. *Int. Sch. Res. Notices*, **2014**, ID 790702.

8. a) Gallardo, H.; Cristiano, R.; Vieira, A. A.; Neves Filho, R. A. W.; Srivastava, R. M.; Bechtold, I. H. *Liq. Cryst*., **2008**, *35* (7), 857 – 863; b) Chidirala, S.; Ulla, H.; Valaboju, A.; Kiran, M. R.; Mohanty, M. E.; Satyanarayan, M. N.; Umesh, G.; Bhanuprakash, K.; Rao, V. J. *J. Org. Chem.*, **2016**, *81* (2), 603 – 614.

9. Mayer, J. C. P.; Sauer, A. C.; Iglesias, B. A.; Acunha, T. V.; Back, D. F.; Rodrigues, O. E. D.; Dornelles, L. *J. Organomet. Chem.*, **2017**, *841*, 1 – 11.

10. a) Gao, C.; Liu, S.-y.; Zhang, X.; Liu, Y.-k.; Qiao, C.-d.; Liu, Z.-e. *Spectrochim. Acta A*, **2016**, *156*, 1 – 8. b) Nozeret, K.; Loll, F.; Cardoso, G. M.; Escudé, C.; Boutorine, A. S. *Biochimie*, **2018**, *149*, 122 – 134. c) Shamsi, F.; Aneja, B.; Hasan, P.; Zeya, B.; Zafaryab, M.; Mehdi, S. H.; Rizvi, M. M. A.; Patel, R.; Rana, S.; Abid, M. *ChemistrySelect*, **2019**, *4* (41), 12176 – 12182.

11. Sheldrick, G. M. *Acta Cryst. A*, **2008**, *64* (1), 112 – 122.

12. Farrugia, L. J. *J. Appl. Crystallogr.* **1997**, *30* (5), 565.

13. a) Bonacorso, H. G.; Calheiro, T, P.; Iglesias, B. A.; Berni, I. R. C.; Silva Junior, E. N.; Rocha, J. B. T.; Zanatta, N.; Martins, M. A. P. *Tetrahedron Letters*, **2016**, *57*, 5017 – 5021; b) Heinrich, G.; S. Schoof, S.; Gusten, H. *J. Photochem.*, **1974**, *3*, 315 – 320.

14. Heller, D. P.; Greenstock, C. L. *Biophysical Chem.*, **1994**, *50*, 305 – 312.

15. Debia, N. P.; Rodríguez, J. J. P.; Silveira, C. H.; Chaves, Iglesias, B. A.; Rodembusch, F. S.; Lüdtke, D. S. *J. Mol. Liq.* **2020**, *309*, 113092.

16. Krüger, R.; Iepsen, B.; Larroza, A. M. E.; Fronza, M. G.; Silveira, C. H.; Bevilacqua, A. C.; Köhler, M. H.; Piquini, P. C.; Lenardão, E. J.; Savegnago, L.; Iglesias, B. A.; Alves, D. *Eur. J. Org. Chem.*, **2020**, *2020* (3), 348 – 361.

17. https://www.wavefun.com/ [accessed in June 2020].

18. Wardell, M.; Wang, Z.; Ho, J. X.; Robert, J.; Ruker, F.; Ruble, J.; Carter, D. C. *Biochem. Biophys. Res. Commun.*, **2002**, *291* (4), 913 – 918.

19. Drew, H. R.; Wing, R. M.; Takano, T.; Broka, C.; Tanaka, S.; Itakura, K.; Dickerson, R. E. *Proc. Natl. Acad. Sci. U.S.A.*, **1981**, *78* (4), 2179 – 2183.

20. https://www.ccdc.cam.ac.uk/solutions/csd-discovery/components/gold/ [accessed in June 2020].

21. https://pymol.org/2/ [accessed in June 2020].

22. Leong, S. W.; Faudzi, S. M. M.; Abas, F.; Aluwi, M. F. F. M.; Rullah, K.; Wai, L. K.; Bahari, M. N. A.; Ahmad, S.; Tham, C. L.; Shaari, K.; Lajis, N. H. *Molecules*, **2014**, *19* (10), 16058 – 16081.

23. Srivastava, R. M.; Pereira, M. C.; Faustino, W. W. M.; Coutinho, K.; Dos Anjos, J. V.; De Melo, S. J. *Monatsh. Chem.*, **2009**, *140* (11), 1319 – 1324.

24. Huguet, F.; Melet, A.; De Sousa, R. A.; Lieutaud, A.; Chevalier, J.; Maigre, L.; Deschamps, P.; Tomas, A.; Leulliot, N.; Page, J. M.; Artaud, I. *ChemMedChem*, **2012**, *7* (6), 1020 – 1030.

25. Huhtiniemi, T.; Suuronen, T.; Rinne, V. M.; Wittekindt, C.; Lahtela-Kakkonen, M.; Jarho, E.; Wallén, E. A. A.; Salminen, A.; Poso, A.; Leppänen, J. *J. Med. Chem.*, **2008**, 51 (15), 4377 – 4380.

26. Stabile, P.; Lamonica, A.; Ribecai, A.; Castoldi, D.; Guercio, G.; Curcuruto, O. *Tetrahedron Lett.*, **2010**, *51*, 4801 – 4805.

27. a) Bonacorso, H. G.; Rodrigues, M. B.; Iglesias, B. A.; Silveira, C. H.; Feitosa, S. C.; Rosa, W. C.; Martins, M. A. P.; Frizzo, C. P.; Zanatta, N. *New J. Chem.*, **2018**, *42* (12), 10024 – 10035. b) Rodrigues, M. B.; Feitosa, S. C.; Wiethan, C. W.; Rosa, W. C.; Silveira, C. H.; Pagliari, A. B.; Martins, M. A. P.; Zanatta, N.; Iglesias, B. A.; Bonacorso, H. G. *J. Fluorine Chem.*, **2019**, *221*, 84 – 90.

28. Li, X.; Cui, X.; Yi, X.; Zhong, S. *J. Mol. Liq.*, **2017**, *241*, 577 – 583.

29. M. Montalti, A. Credi, L. Prodi, M.T. Gandolfi, Handbook of Photochemistry. 3rd ed. CRC Press, Taylor & Francis; 2006.

30. Meng, X.-Y.; Zhang, H.-X.; Mezei, M.; Cui, M. *Curr. Comput. Aided Drug Des.* **2011**, *7* (2), 146 – 157.

31. Husain, M. A.; Ishqi, H. M.; Sarwar, T.; Rehman S. U.; Tabish, M. *Med. Chem. Commun.*, **2017**, *8*, 1283 – 1296.

32. Laskar, K.; Alam, P.; Khan, R. H.; Rauf, A. *Eur. J. Med. Chem.*, **2016**, *122*, 72 – 78.

DOI: 10.1039/D0NJ04530F

Table of Contents

Synthesis, spectroscopic characterization and DNA/HSA binding study of (phenyl/naphthyl)ethenyl-substituted 1,3,4-oxadiazolyl-1,2,4-oxadiazoles

João C. P. Mayer,[a] Thiago V. Acunha,[b] Oscar E. D. Rodrigues,[a] Davi F. Back,[c] Otávio Augusto Chaves,[d] Luciano Dornelles[a]* and Bernardo A. Iglesias[b]**

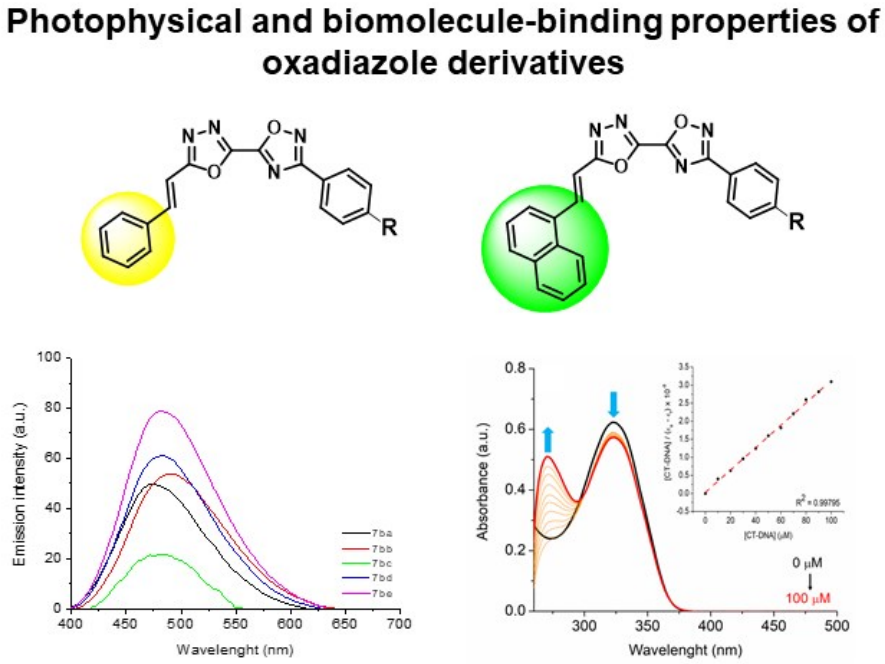

Novel 1,3,4-oxadiazolyl-1,2,4-oxadiazole derivatives with promising photophysical and DNA/HSA-binding properties are reported.